# Deformation of continental crust along a transform boundary, Coast Mountains, British Columbia

Margaret E. Rusmore,[1] Scott W. Bogue,[1] Karen Dodson,[1] Kenneth A. Farley,[2] and Glenn J. Woodsworth[3]

Received 23 March 2009; revised 23 February 2010; accepted 2 March 2010; published 17 July 2010.

[1] New structural, paleomagnetic, and apatite (U-Th)/He results from the continental margin inboard of the Queen Charlotte fault (~54°N) delineate patterns of brittle faulting linked to transform development since ~50 Ma. In the core of the orogen, ~250 km from the transform, north striking, dip-slip brittle faults and vertical axis rotation of large crustal domains occurred after ~50 Ma and before intrusion of mafic dikes at 20 Ma. By 20 Ma, dextral faulting was active in the core of the orogen, but extension had migrated toward the transform, continuing there until <9 Ma. Local tilting in the core of the orogen is associated with glacially driven, post-4 Ma exhumation. Integration with previous results shows that post-50 Ma dextral and normal faulting affected a region ~250 km inboard of the transform and ~300 km along strike. Initially widespread, the zone of active extension narrowed and migrated toward the transform ~25 Ma after initiation of the transform, while dextral faulting continued throughout the region. Differential amounts of post-50 Ma extension created oroclines at the southern and northern boundaries of the deformed region. This region approximately corresponds to continental crust that was highly extended just prior to transform initiation. Variation in Neogene crustal tilts weakens interpretations relying on uniform tilting to explain anomalous paleomagnetic inclinations of mid-Cretaceous plutons. Similarities to the Gulf of California suggest that development of a transform in continental crust is aided by previous crustal extension and that initially widespread extension narrows and moves toward the transform as the margin develops. **Citation:** Rusmore, M. E., S. W. Bogue, K. Dodson, K. A. Farley, and G. J. Woodsworth (2010), Deformation of continental crust along a transform boundary, Coast Mountains, British Columbia, *Tectonics*, *29*, TC4007, doi:10.1029/2009TC002502.

## 1. Introduction

[2] Formation of a transform margin through interaction of a spreading ridge and continental convergent margin profoundly alters the continental plate. Effects may include cessation of the arc magmatism, inception of forearc magmatism, crustal extension, and localization of the transform within the continental plate. In some cases, the transform steps inboard, transferring a sliver of continental crust to the oceanic plate and truncating the continental margin. Along western North America, two great transform faults have formed in this fashion during the Tertiary: the San Andreas fault-Gulf of California system and the Queen Charlotte transform in British Columbia and southeastern Alaska. In both cases, extension affected the continental crust inboard of the initial plate boundary, forming marine basins along parts of the continental margin. The transform faults ultimately transferred slices of continental crust to the oceanic plates. These broad similarities suggest that such transform boundaries may develop through a common kinematic progression, but key aspects of the deformation of the continental edge are debated in Baja California and incompletely known in British Columbia.

[3] The distribution of strain within the continental margin is probably the most uncertain element of the kinematic history in both margins, although it is far better documented around the Gulf of California than in British Columbia. Most models for the Gulf of California show fully partitioned strain, analogous to obliquely convergent margins [e.g., *Lonsdale*, 1989; *Oskin and Stock*, 2003; *Spencer and Normark*, 1979; *Stock and Hodges*, 1989; *Umhoefer et al.*, 2002]. The extensional component of plate motion would have been taken up by rifting in the extinguished arc, while strike-slip translation was accommodated along the site of the former trench. As the margin matured dextral slip shifted into the Gulf, forming the present configuration of long transforms joining smaller rift basins and feeding into the San Andreas fault system of southern California. Recent work downplays the partitioning of strain, proposing integrated strike-slip and normal faulting in the Gulf from inception of the transform [*Fletcher et al.*, 2007]. In this kinematic model, dextral slip along the inboard fault system is about 150 km greater than in the more strongly partitioned scenario, requiring greater translation for the Baja peninsula and greater total slip on faults within the continent.

[4] Like the Gulf of California, the Queen Charlotte Basin formed through linked strike-slip and normal faulting driven by the transform boundary [*Hollister et al.*, 2008; *Lewis et al.*, 1991; *Morozov et al.*, 1998; *Rohr and Dietrich*, 1991; *Rohr and Currie*, 1997; *Rohr and Dietrich*, 1992]. Normal fault-

[1]Department of Geology, Occidental College, Los Angeles, California, USA.
[2]Division of Geological and Planetary Sciences, California Institute of Technology, Pasadena, California, USA.
[3]Geological Survey of Canada, Vancouver, British Columbia, Canada.


0278-7407/10/2009TC002502

ing coeval with transform motion has been recognized in a few places on the mainland east of the basin [*Butler et al.*, 2001a; *Davidson et al.*, 2003; *Evenchick et al.*, 1999] which *Hollister et al*. [2008] link to development of the transform margin. Latest Miocene and younger volcanism and faulting is interpreted as the signal of incipient Basin and Range style rifting inboard of the continental margin during the last 10 Ma [*Edwards and Russell*, 1999; *Edwards and Russell*, 2000]. These observations raise the possibility that, similar to the Gulf of California, widespread extension affected the continental margin far inboard of the Queen Charlotte fault.

[5] Potentially large extension of the continental margin would affect paleogeographic reconstructions for western North America. The long-running Baja BC controversy [e.g. *Butler et al.*, 2001b; *Cowan et al.*, 1997; *Irving*, 1985; *Irving et al.*, 1985; *Mahoney et al.*, 1999], centers on the interpretation of anomalously shallow paleomagnetic inclinations from Cretaceous plutons and volcanics in western British Columbia. Interpreted as indications of paleolatitude, these inclinations would indicate 2500–3000 km of northward translation of western British Columbia since circa 90 Ma. This large translation is at least 1000 km greater than can be reconciled with even the most mobilistic geological reconstructions [*Wyld et al.*, 2006]. Alternatively, unrecognized tilting of the plutons down to southwest would decrease the amount of transport implied by the paleomagnetic data. Recognizing that significant crustal tilting might accompany basin opening, *Butler et al.* [2006] infer 10–15° of uniformly northeast side-up tilting of plutons on the eastern flank of the Queen Charlotte Basin. In this model, the Neogene tilting would follow ~30° of Late Cretaceous to Eocene tilting. The combined tilting would obviate the need for any northward transport of western British Columbia. *Butler et al.* [2006] call for further study of the eastern flank of the basin, especially with low-temperature geothermometry, to assess the prevalence of northeast side-up tilting.

[6] In this study, we examine the extent, timing, and style of Neogene deformation along the eastern flank of the Queen Charlotte Basin through structural, paleomagnetic, and apatite (U-Th)/He studies. The long history of the transform margin allows tracking of strain patterns through time and space as the margin matured. Our results provide insight into the effects of transform faults on continental margins and on the Baja BC controversy.

## 2. Geological Setting

[7] The Queen Charlotte transform boundary began to form when either the Kula or Resurrection spreading ridges approached the subduction zone along British Columbia and SE Alaska in early Tertiary time [*Engebretson et al.*, 1985; *Hyndman and Hamilton*, 1991; *Lonsdale*, 1988; *Madsen et al.*, 2006; *Stock and Molnar*, 1988]. Because most of the marine record of these plates has been obliterated during subduction, the ridge position, plate velocities, and even the existence of various plates are difficult to ascertain. All reconstructions agree, however, that in early Tertiary time either the Kula or Resurrection plate was subducting beneath British Columbia and that a ridge encountered the trench shortly after 50 Ma. Formation of the transform boundary truncated the continental margin, removing the accretionary complex and cutting into previously accreted terranes, such as Wrangellia, now exposed on the Queen Charlotte Islands. The Queen Charlotte Islands mark the only area on the >1200 km long transform where the continental margin subsided to form a marine basin, the Queen Charlotte Basin (Figure 1). The record of magmatism, deformation, and basin subsidence shows that formation of the Queen Charlotte Basin is linked to the adjacent transform margin [*Hollister et al.*, 2008; *Lewis et al.*, 1991; *Morozov et al.*, 1998; *Rohr and Dietrich*, 1991; *Rohr and Currie*, 1997; *Rohr and Dietrich*, 1992]. Initiation of the transform is signaled by forearc volcanism attributed to slab windows along the continental margin [*Breitsprecher et al.*, 2003; *Haeussler et al.*, 2003; *Hyndman and Hamilton*, 1991; *Madsen et al.*, 2006; *Matmon et al.*, 2006].

[8] Previous studies focused on the marine basin, the Queen Charlotte Islands, and on the mainland around Prince Rupert (Figure 1). These studies revealed Neogene faulting, crustal tilting, and mafic to felsic magmatism. The oldest Tertiary magmatism in the Queen Charlotte Islands is 46–39 Ma [*Anderson and Reichenbach*, 1991], but most magmatism in the Queen Charlotte Islands is ~25–20 Ma, coincident with the main phase of basin formation [*Hickson*, 1991; *Rohr and Dietrich*, 1992; *Souther and Jessop*, 1991]. Mafic dikes are widespread in the islands and on the mainland; sparse dating shows they range from ~40 to <22 Ma [*Crawford et al.*, 2005; *Evenchick et al.*, 1999; *Hutchison*, 1982; *Irving et al.*, 1992; *Souther and Jessop*, 1991]. Paleomagnetic study of the dikes on Queen Charlotte Island shows 9°–16° of tilting down to the north or northwest as the result of Eocene and younger extension [*Irving et al.*, 1992].

[9] Within the marine basin, seismic reflection data reveal continental crust extensively disrupted by north and northwest striking faults [*Hollister et al.*, 2008; *Lewis et al.*, 1991; *Morozov et al.*, 2001, 1998; *Rohr and Dietrich*, 1991; *Rohr and Currie*, 1997; *Rohr and Dietrich*, 1992]. Half-grabens and rarer grabens are filled with Lower Miocene volcanic rocks overlain by syn-rift middle to Upper Miocene sedimentary strata capped by Pliocene sediments that are generally post-rift [*Rohr and Dietrich*, 1992]. Low-angle reflectors are interpreted as young west dipping ductile shear zones that formed the mid-crustal parts of this system [*Hollister et al.*, 2008] and help delineate a large graben offshore from Prince Rupert (Figure 1). Neogene brittle faults and crustal tilting are recognized in a few places east of Prince Rupert [*Butler et al.*, 2001a; *Davidson et al.*, 2003; *Evenchick et al.*, 1999] (Figure 1).

[10] Thermal modeling suggests extension was nearly uniform throughout most of the Queen Charlotte Basin, with net extension of ~76%, or about 50 km, mostly between 20 and 25 Ma [*Dehler et al.*, 1997]. The northeastern margin of the basin records at least 30% extension [*Hollister et al.*, 2008]. Following extension, the northern part of the margin became slightly transpressive, with about 10–15 km of underthrusting [*Prims et al.*, 1997] and moderate contrac-

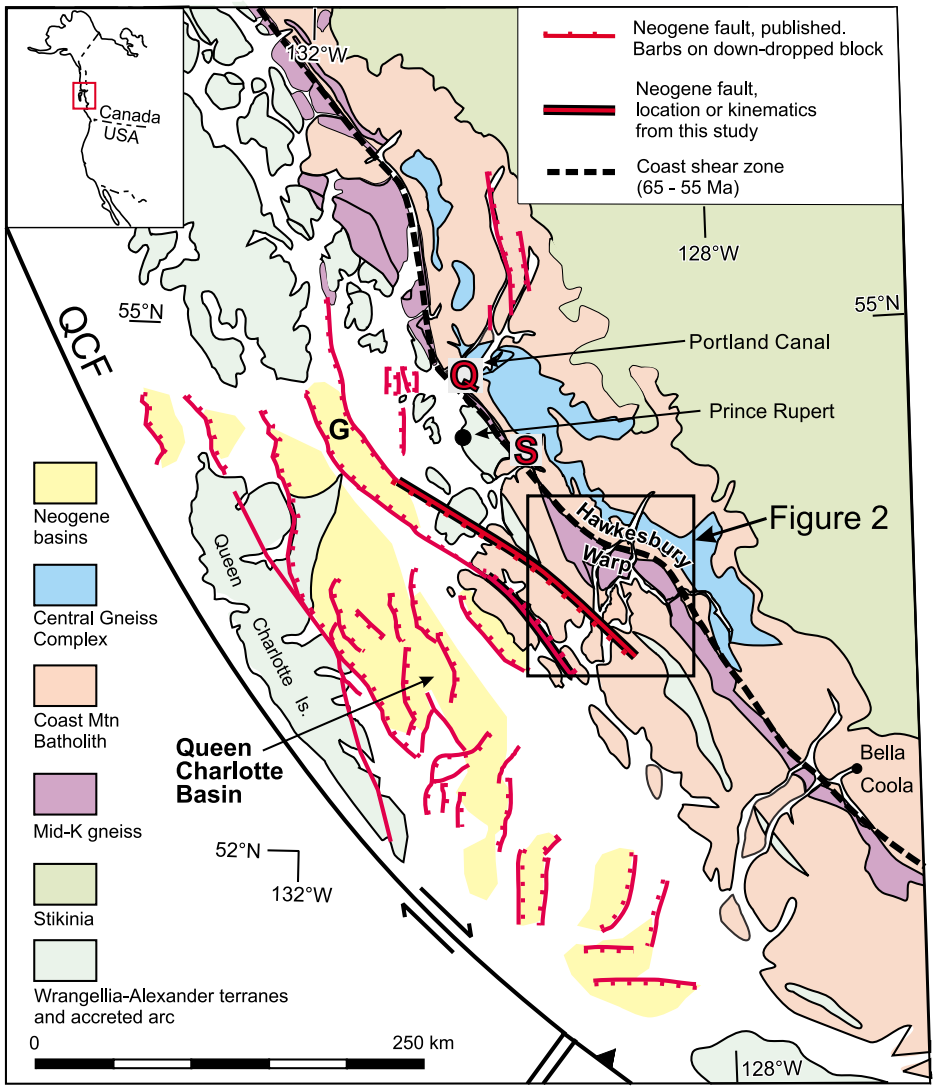


**Figure 1.** Simplified geologic map of Coast Mountains Batholith and Queen Charlotte Basin (Neogene fill shown in yellow). **G**, shows graben from the work of *Hollister et al.* [2008]; **S**, site of brittle fault study by *Davidson et al.* [2003]; **Q**, location of paleomagnetic study by *Butler et al.* [2001a]; QCF, Queen Charlotte fault. Geology modified from the works of *Hollister et al.* [2008], *Rohr and Dietrich* [1992], and *Wheeler and McFeely* [1991].

tion in both plates adjacent to the Queen Charlotte fault [*Rohr et al.*, 2000].

## 3. Methods

### 3.1. Field Methods

[11] Fieldwork was focused on Douglas Channel with additional reconnaissance in the islands southwest of the channel and south along Gardner Canal (Figures 2, 3, and 4 and Table A1). Plutonic rocks (mainly tonalite) were sampled for (U-Th)/He in apatite (AHe) dating from sites spaced 1–5 km apart (Figure 2) along Douglas Channel. More widely spaced AHe samples were collected from the islands southwest of Douglas Channel; all but one sample are from sea level. Dikes and brittle faults were mapped in detail at scales ~1:10,000 or greater along the northwestern shore of Douglas Channel (Figure 3). Mapping was completed by walking all available shoreline and by using a skiff to search areas inaccessible on foot. Excellent exposures provide access to more than three quarters of the shoreline, so most brittle faults and dikes were probably observed. In areas where few dikes or faults were found on the northwestern shores of Douglas Channel, the southeastern shore was also mapped. Locations were recorded with a hand-held GPS.

[12] Thirty-one sites were sampled for paleomagnetic study: 19 from the Paleocene Quottoon pluton and 12 from the mafic dikes (Figure 4). Samples were only collected where the rock appeared unstrained and where the attitude of a widespread magmatic foliation [*Rusmore et al.*, 2001]

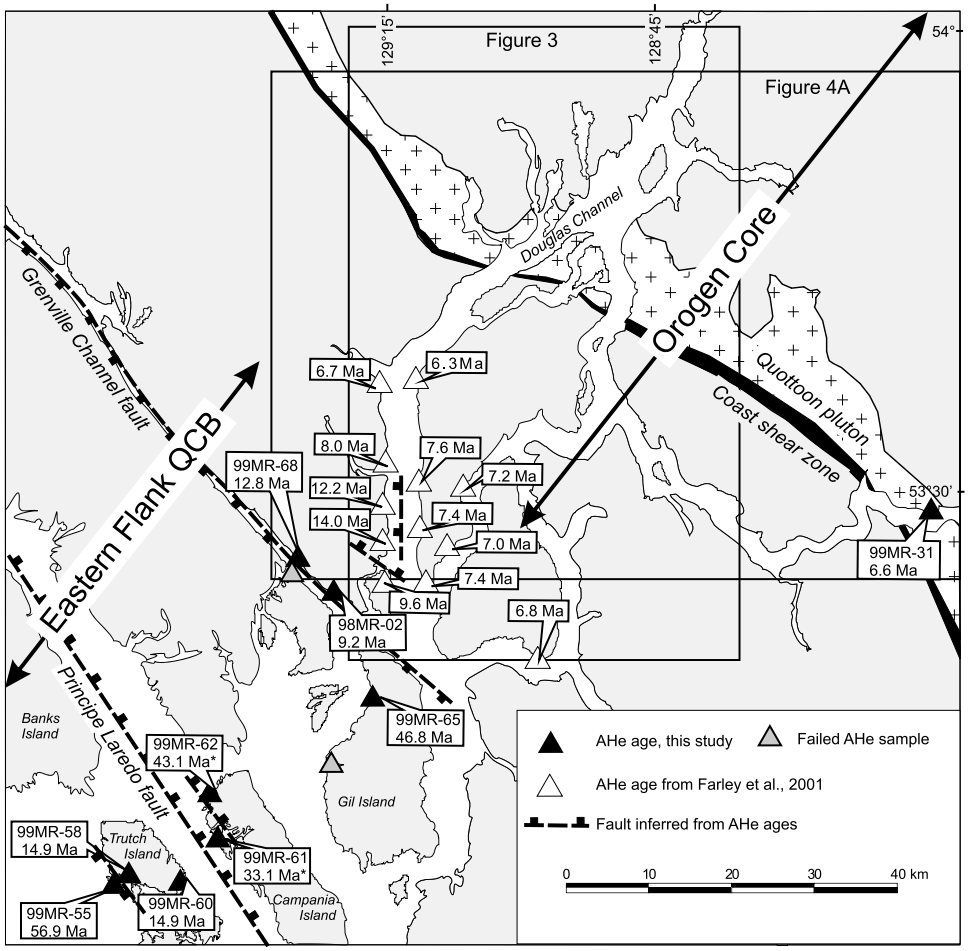


**Figure 2.** Map of apatite (U-Th/He) ages and inferred faults. Boxes mark locations of Figures 3 and 4A. Asterisk denotes samples with He age-grain size correlation; mean age is reported. Eastern Flank QCB (Queen Charlotte Basin) and Orogen Core are regions discussed in text.

was easily measurable. Core samples (seven per site, typically at several meter spacing) were collected using a gasoline-powered portable rock drill and oriented using a sun compass. In the few instances where a sun shadow was unavailable, core orientations and the local geomagnetic declination were measured with a magnetic compass.

### 3.2. Apatite (U-Th)/He Methods

[13] Apatites were separated using standard rock crushing, magnetic, and heavy liquids techniques. Grains selected for dating were handpicked under a binocular microscope to be free of visible inclusions and grain dimensions measured for $\alpha$ ejection correction [*Farley et al.*, 1996]. Early dating analyses followed the technique of *Farley et al.* [2001] in which four grains were combined and He extracted using a resistance furnace. Later analyses were performed on single grains using the procedure described by *House et al.* [2000]. In both cases, He was measured by isotope dilution quadrupole mass spectrometry after cryofocusing and purification. Apatites were retrieved from the vacuum line, dissolved in $HNO_3$, spiked with $^{235}U$ and $^{230}Th$, and measured for U and Th on an Element-1 inductively coupled plasma mass spectrometer. On several samples, both furnace and laser analyses were performed, verifying good agreement between the two methods. The propagated analytical uncertainty on individual ages is about 3%. However as shown in Table 1, ages do not reproduce at this level. In some cases, there are age-grain size correlations, which explain some of the observed variability. The presence of such correlations and the small size of this data set make it difficult to independently estimate the true precision of individual ages. Based on larger data sets from rocks of similar age and lithology in the Coast Mountains and the Sierra Nevada [*Clark et al.*, 2005; *Ehlers et al.*, 2006; *Mahéo et al.*, 2009], we infer a precision of ~10%. We therefore compute mean ages and adopt $1\sigma$ uncertainties of 10%/sqrt($N$) where $N$ is the number of replicates performed.

### 3.3. Paleomagnetic Methods

[14] The remanence of short (1–2.5 cm) specimens cut from 2.5 cm diameter cores was analyzed using commercial rock magnetometers (both fluxgate spinner and cryogenic)

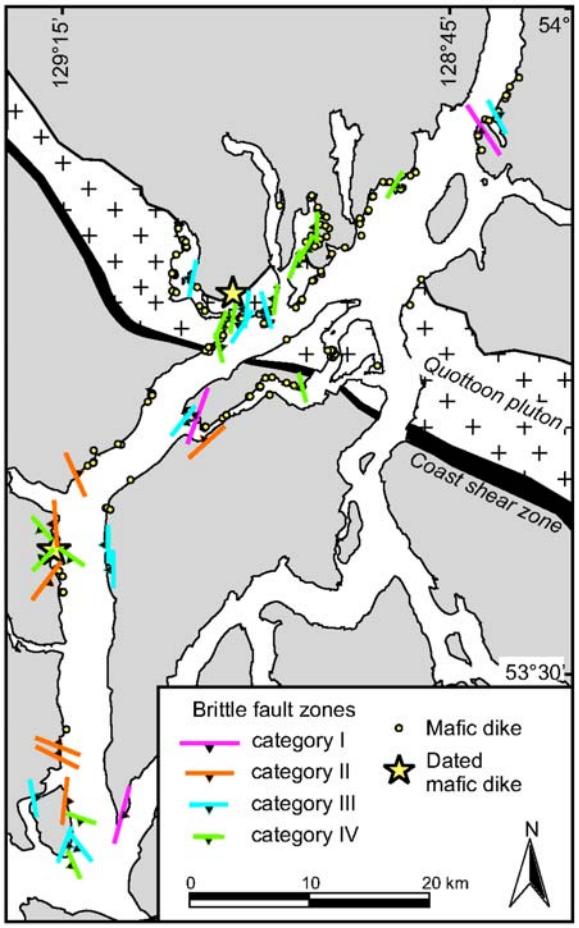


**Figure 3.** Map showing dikes and location, size category, and orientation of brittle fault zones on Douglas Channel (modified from *Roddick* [1970] and *Rusmore et al.* [2001]).

and demagnetization devices (both alternating field (AF) and thermal). All remanence components were determined by fitting lines to linear segments on orthogonal vector demagnetization plots [*Kirschvink*, 1980].

## 4. Results

### 4.1. Apatite (U-Th)/He Ages

[15] Apatite (U-Th)/He ages for much of Douglas Channel were previously reported [*Farley et al.,* 2001] and a subset of those from sea level are plotted on Figure 2. These ages range from 6 to 14 Ma. Here we present eight new ages collected closer to the transform margin and one within the core of the range on Gardner Canal (Figure 2 and Table 1).

[16] A single analysis from Gardner Canal, the eastern-most locality in this study, produced the youngest new AHe age of 6.6 Ma (99 MR-31). This age is consistent with previously published AHe ages on the northern and eastern parts of Douglas Channel.

[17] Moving progressively further to the south and west of the previous data set, the ages become generally older and more spatially variable. Two tonalite samples from the northeast shore of Grenville Channel yielded ages of 12.8 Ma (99MR-68) and 9.2 Ma (98MR-02). Quartz diorite (99MR-65) from Gil Island yielded an age of 46.8 Ma.

[18] Two samples of leucocratic tonalite from Campania Island were dated using multiple grain size fractions. *Roddick* [1970] shows the samples as belonging to one plutonic unit, and the hand samples are very similar. Apatite grains from the samples have identical chemistry, supporting field observations that the samples are from one pluton. With the exception of one grain, ages from both samples are correlated with grain size (Figure 5) and grains from the northern sample, 99MR-62, are about 10 Ma younger than similar size grains in the southern sample, 99MR-61. The pattern on Figure 5 suggests that the samples cooled slowly

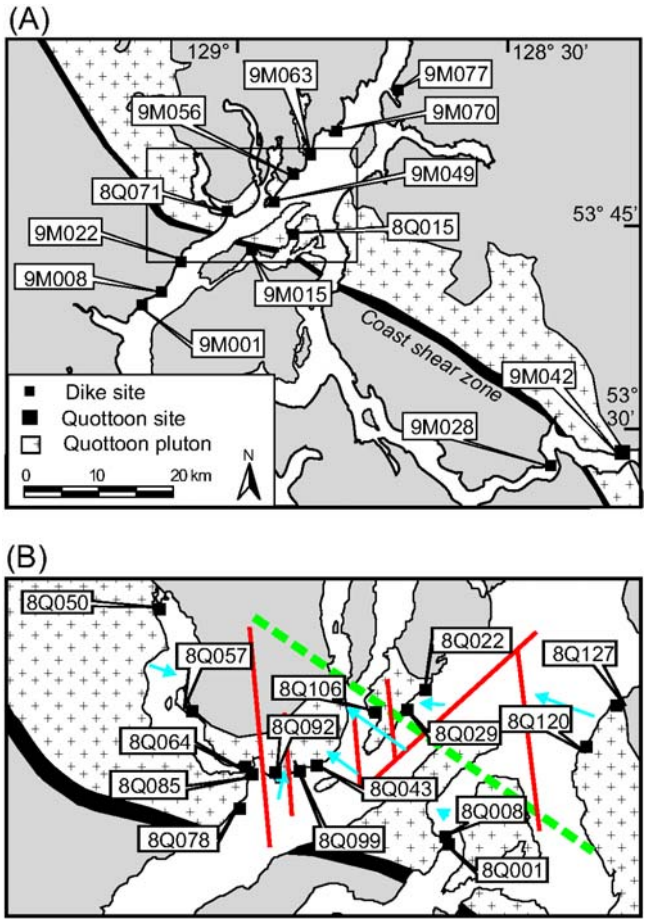


**Figure 4.** Locations of paleomagnetic sample sites and inferred crustal domains. (a) Sites in mafic dikes and southern Quottoon pluton. Box shows location of Figure 4b. (b) Sites in Quottoon pluton on Douglas Channel and structural interpretation discussed in section 5.1.1. Broken green line is rotation domain boundary; solid red lines are inferred tilt domain boundaries. Blue arrows point toward up-tilted end of tilt blocks; length of arrow is proportional to amount of tilt, which ranges from 2° to 39°.

**Table 1.** Data for (U-Th)/He Apatite Geochronology

| | Sample | Raw Age (Ma) | Corrected Age (Ma) | ±1 $\sigma$ | U (ppm) | Th (ppm) | He (nmol/g) | Mass ($\mu$g) | Ft | Prism Half-Width ($\mu$m) | Prism Length ($\mu$m) |
|---|---|---|---|---|---|---|---|---|---|---|---|
| **Gardner Canal** | | | | | | | | | | | |
| ***99 MR-31*** | furnace-4 gr | 5.5 | ***6.6*** | ***0.7*** | 9.1 | 12.4 | 8.06 | | 0.83 | | |
| **Grenville Channel** | | | | | | | | | | | |
| ***98 MR-02*** | furnace-4 gr | 7.2 | ***9.2*** | ***0.9*** | 11.0 | 11.2 | 0.53 | | 0.78 | | |
| ***99 MR-68*** | a | 8.3 | 11.7 | | 11.1 | 9.7 | 0.61 | 2.80 | 0.71 | 40 | 326 |
| | b | 11.3 | 14.0 | | 6.9 | 4.0 | 0.48 | 6.55 | 0.80 | 63 | 309 |
| | c* | 6.3 | 7.8 | | 6.9 | 11.6 | 0.33 | 6.36 | 0.80 | 63 | 300 |
| | d | 9.9 | 12.1 | | 6.3 | 2.6 | 0.37 | 7.04 | 0.82 | 71 | 257 |
| | e | 8.8 | 11.5 | | 11.6 | 4.8 | 0.61 | 4.87 | 0.77 | 51 | 343 |
| | f | 9.9 | 12.9 | | 9.6 | 4.7 | 0.58 | 4.87 | 0.77 | 51 | 343 |
| | g | 11.8 | 15.1 | | 4.8 | 2.1 | 0.34 | 4.81 | 0.78 | 57 | 274 |
| | h | 9.5 | 11.8 | | 8.2 | 3.2 | 0.47 | 7.27 | 0.81 | 63 | 343 |
| | i | 10.1 | 12.6 | | 7.5 | 4.9 | 0.48 | 7.62 | 0.80 | 60 | 394 |
| | j* | 23.0 | 28.3 | | 7.7 | 3.3 | 1.06 | 8.55 | 0.81 | 63 | 403 |
| | furnace-4 gr | 10.9 | 13.8 | | 8.4 | 5.6 | 0.58 | | 0.79 | | |
| | | ***mean*** | ***12.8*** | ***0.4*** | | | | | | | |
| **Gil Island** | | | | | | | | | | | |
| ***99 MR-65*** | b | 35.1 | 47.7 | | 55.4 | 88.4 | 14.57 | 2.94 | 0.74 | 45 | 270 |
| | c | 41.6 | 56.1 | | 54.0 | 116.7 | 18.48 | 2.67 | 0.74 | 48 | 216 |
| | d | 31.6 | 39.7 | | 90.9 | 112.0 | 20.16 | 5.92 | 0.80 | 60 | 306 |
| | furnace-4 gr | 32.1 | 43.8 | | 104.0 | 118.0 | 23.00 | | 0.73 | | |
| | | ***mean*** | ***46.8*** | ***2.3*** | | | | | | | |
| **Campania Island** | | | | | | | | | | | |
| ***99 MR-61*** | a | 31.9 | 44.7 | | 5.5 | 3.8 | 1.11 | 2.32 | 0.71 | 47 | 194 |
| | b | 25.4 | 37.4 | | 5.0 | 3.2 | 0.80 | 1.98 | 0.68 | 39 | 242 |
| | c | 25.5 | 38.1 | | 6.0 | 3.8 | 0.96 | 1.55 | 0.67 | 39 | 189 |
| | d | 17.2 | 27.6 | | 3.8 | 3.5 | 0.43 | 1.30 | 0.62 | 32 | 235 |
| | e | 16.8 | 23.4 | | 7.4 | 2.7 | 0.73 | 2.14 | 0.71 | 48 | 170 |
| | furnace-4 gr | 19.3 | 27.1 | | 8.2 | 2.9 | 0.93 | | 0.71 | | |
| | | | ***33.1*** | | ***grain size correlation*** | | | | | | |
| ***99MR-62*** | a | 38.6 | 49.0 | | 5.8 | 4.2 | 1.43 | 7.29 | 0.79 | 62 | 355 |
| | b | 32.5 | 41.2 | | 4.1 | 1.3 | 0.78 | 6.68 | 0.79 | 62 | 321 |
| | c | 26.9 | 36.2 | | 6.0 | 3.3 | 0.99 | 3.63 | 0.74 | 52 | 251 |
| | d | 30.6 | 40.0 | | 5.5 | 2.6 | 1.02 | 5.19 | 0.76 | 55 | 319 |
| | furnace-4 gr | 41.0 | 49.4 | | 4.2 | 1.5 | 1.02 | | 0.83 | | |
| | | | ***43.14*** | | ***grain size correlation*** | | | | | | |
| **Trutch Island** | | | | | | | | | | | |
| ***99MR-55*** | a | 43.9 | 51.4 | | 17.9 | 38.3 | 6.43 | 14.09 | 0.85 | 90 | 324 |
| | b | 55.5 | 68.7 | | 22.1 | 38.0 | 9.42 | 6.53 | 0.81 | 66 | 279 |
| | c | 48.8 | 57.8 | | 7.1 | 19.2 | 3.10 | 12.68 | 0.84 | 81 | 360 |
| | d | 52.5 | 61.0 | | 15.4 | 31.3 | 6.51 | 18.01 | 0.86 | 90 | 414 |
| | furnace-4 gr | 42.9 | 52.4 | | 17.4 | 33.5 | 5.91 | | 0.82 | | |
| | furnace-4 gr | 39.8 | 50.4 | | 18.1 | 34.5 | 5.68 | | 0.79 | | |
| | | ***mean*** | ***56.9*** | ***2.3*** | | | | | | | |
| ***99 MR-58*** | furnace-4 gr | 10.90 | ***14.9*** | ***1.5*** | 17.3 | 23.3 | 1.35 | | 0.73 | | |
| ***99 MR-60*** | furnace-4 gr | 12.2 | ***14.9*** | ***1.5*** | 22.4 | 29.4 | 1.94 | | 0.82 | | |

between about 50 and 23 Ma, such that small differences in closure temperature associated with grain size variations are amplified into large age differences [*Reiners and Farley*, 2001].

[19] Sea-level AHe ages differ significantly across Trutch Island: 99MR-60 from the eastern shore produced an age of 14.9 Ma, whereas 99MR-55 on the western shore yielded an age of 56.9 Ma. Sample 99MR-58 from 297 m elevation gave an AHe age of 14.9 Ma.

### 4.2. Dikes

[20] Widespread dikes are dark brown to greenish black, planar, and range from ~5 cm to 10 m thick, with an average width of 1 m. The thickest dikes are typically sheeted. Most dikes have fine-grained chilled margins; vesicles and amygdules occur in the centers of some dikes. Rare phenocrysts are hornblende, biotite, and plagioclase. Hornblende and biotite phenocrysts generally appear fresh in thin

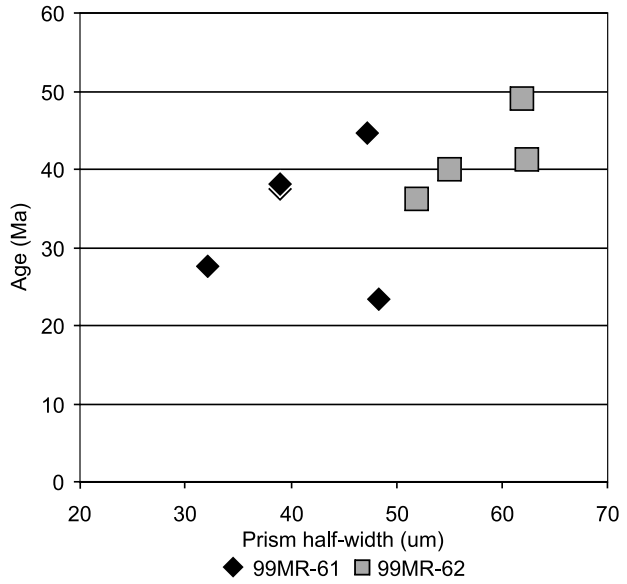


**Figure 5.** AHe ages on the two samples from Campania Island. Unique among the dataset, these two samples show grain size-age correlations suggesting slow cooling [*Reiners and Farley*, 2001]. For a given grain size, apatites from 99 MR-61 are older than those from 99 MR-62.

section; plagioclase is commonly altered to saussurite and calcite. The groundmass of most samples contains alteration products such as very fine grained calcite, chlorite, clays or zeolites, pyrite, and oxides. Based on their dark color, most dikes are likely basalt, but those that are lighter colored and especially those with hornblende and biotite phenocrysts are probably andesite. For simplicity, we refer to the all the dikes as "mafic."

[21] Two hundred thirty-one mafic dikes were mapped along Douglas Channel (Figure 3). They are most abundant in the northern two thirds of Douglas Channel and are nearly absent for ~15 km in the southern channel. Very few dikes were found during reconnaissance of the islands southwest of Douglas Channel and along Gardner Canal. No correlation between dike width and location is apparent in GIS analysis of the dikes, and nowhere did the dikes accommodate much extension. Even on short (3–5 km) transects where dikes are most abundant, dike-related extension was only 2%–3%. Measured across the 60 km transect where dikes occur, the strain is insignificant.

[22] The dikes are steeply dipping and most strike NE–SW with an average orientation of 236, 79°NW (Figure 6). Contoured data shows no statistically significant subpopulations. Despite this general homogeneity of orientations, two geographically restricted subsets can be identified on the basis of either strike or dip. Both occur along Douglas Channel northeast of the Coast shear zone. One subset comprises 29 dikes with dips <60°. Most of these dikes dip NW and their average strike is 226°, similar to the whole population. As discussed below, the shallower dips are caused by later structural disruption. Fourteen northwest striking dikes (324°–360°) also occur only in this area but do not have dips gentler than the main population. Mafic dikes with similar NNW orientations are common northeast of the north end of the channel, where they cut a 14 Ma pluton (G. Woodsworth, unpublished mapping). Perhaps the NW striking dikes on Douglas Channel are the southern edge of that dike swarm. Except for these few NW striking dikes, the mafic dikes appear to be a single NE striking swarm.

[23] Ar-Ar dating of two dikes with typical orientations yielded Early Miocene ages (Figure 3). From the southern part of the channel, 99MR-03 is a grayish green dike 140 cm wide oriented 217, 86°NW. A 40Ar/39Ar age of 21.78 ± 0.03 Ma was determined by the Berkeley Geochronology Center from a 13 step plateau comprising >95% of the total 39Ar (Table 2) on optically fresh hornblende phenocrysts. A similar age was obtained from a dike about 25 km to the northeast (Figure 3). The dark greenish brown dike is 35–40 cm thick, strikes 219, and dips 86°NW. Several thin NW striking, near-vertical dextral brittle faults cut the dike. Ar-Ar dating of unaltered hornblende phenocrysts produced an age of 19.2 ± 0.8 Ma (M. Villeneuve, written communication, 2004). Both dikes intruded rocks that had previously cooled below biotite and hornblende blocking temperatures [*Friedman et al.*, 2001; *Gareau*, 1991; *Roddick*, 1970; *Rusmore et al.*, 2005] so the Ar-Ar ages are interpreted as the intrusive ages of the dikes. The homogeneity of dike orientations and the similarity of the ages from the two widely separated dikes lead us to infer that most of the mafic dikes along Douglas Channel are about 20 Ma old.

### 4.3. Brittle Faults

[24] Brittle faults are present along most of Douglas Channel except in the southern ~15 km (Figure 3) where dikes are also nearly absent. Fault-related lineations are rare because intense wave-driven erosion preferentially scours away slickensides. Faults range from individual faults a few millimeters across to well-developed fault zones many meters wide. The largest fault zones commonly coincide with topographic lineaments more than a kilometer long.

[25] To provide consistent comparisons of faults, each was ranked by width of the fault zone and the development of fault-related features within the zone. The largest fault zones, grade I, are many meters wide and marked by pervasively altered and variably cataclastic rocks with many individual fault surfaces. The alteration is commonly both red (hematitic) and green (chloritic). These faults zones have a strongly deformed central zone flanked by less deformed rocks. Cataclastic rocks include widely developed cataclastic breccias, meter-scale layers of foliated and unfoliated cataclastic rocks, and ultracataclastic rock bands thicker than 10 cm. Faults ranked as grades II, III, and IV are progressively narrower zones, but all contain ultracataclastic rocks and multiple fault surfaces. Individual fault surfaces within fault zones I–IV are generally subparallel to each other and we interpret them as kinematically linked. The smallest faults, grade V, are isolated faults a few millimeters wide. They appear quite insignificant in the field, although displacements of 1–2 m were observed on two of these faults.

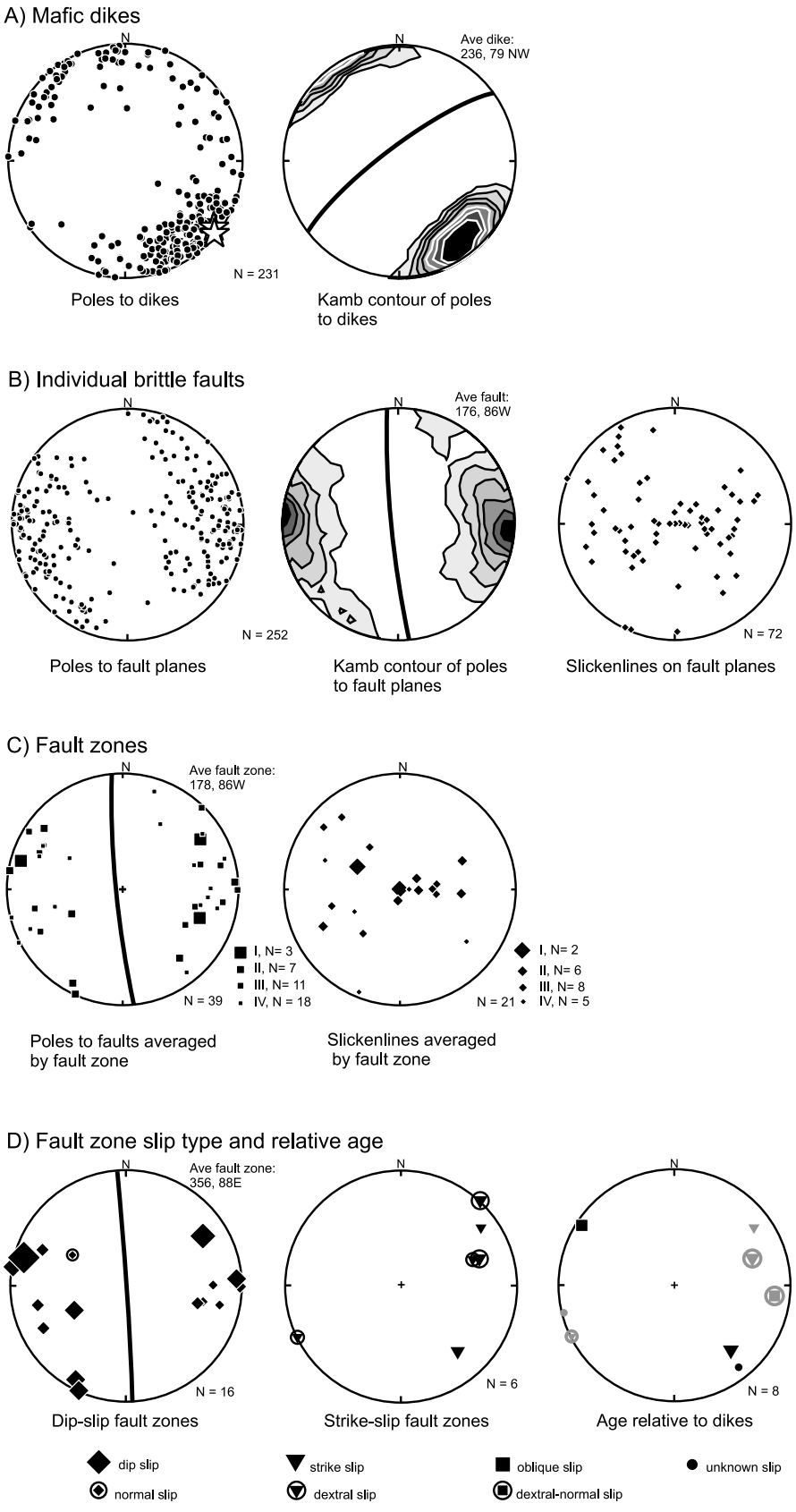
A) Mafic dikes
N
N = 231
Poles to dikes
N
Ave dike:
236, 79 NW
Kamb contour of poles
to dikes
B) Individual brittle faults
N
N = 252
Poles to fault planes
N
Ave fault:
176, 86W
Kamb contour of poles
to fault planes
N
N = 72
Slickenlines on fault planes
C) Fault zones
N
Ave fault zone:
178, 86W
I, N= 3
II, N= 7
III, N= 11
IV, N = 18
N = 39
Poles to faults averaged
by fault zone
N
I, N= 2
II, N= 6
III, N= 8
IV, N = 5
N = 21
Slickenlines averaged
by fault zone
D) Fault zone slip type and relative age
N
Ave fault zone:
356, 88E
N = 16
Dip-slip fault zones
N
N = 6
Strike-slip fault zones
N
N = 8
Age relative to dikes
dip slip
normal slip
strike slip
dextral slip
oblique slip
dextral-normal slip
unknown slip

**Figure 6**

**Table 2.** Data for 40Ar/39Ar Geochronology on 99MR-03

| Step | Age | ±Error | Cumulative %39 | %Rad | Ca/K | Cl/K |
|---|---|---|---|---|---|---|
| A | 3.66 | 3.883 | 0.1 | 54.3 | 0.00E+00 | 4.08E-02 |
| B | 40.21 | 4.430 | 0.4 | 28.8 | 1.10E+00 | 2.60E-02 |
| C | 26.66 | 1.871 | 0.8 | 31.6 | 1.04E+00 | 8.72E-03 |
| D | 19.69 | 1.925 | 1.3 | 21.3 | 5.96E-01 | 2.25E-02 |
| E | 21.96 | 4.020 | 1.6 | 15.6 | 1.25E+00 | 6.64E-03 |
| F | 23.16 | 3.117 | 1.8 | 23.8 | 2.62E+00 | 3.85E-03 |
| G | 18.06 | 1.977 | 2.0 | 28.1 | 8.64E+00 | 1.68E-02 |
| H | 21.86 | 0.653 | 2.7 | 65.0 | 1.41E+01 | 1.09E-02 |
| I | 21.54 | 0.203 | 4.9 | 85.5 | 1.52E+01 | 6.82E-03 |
| J | 21.75 | 0.095 | 10.2 | 93.8 | 1.53E+01 | 4.45E-03 |
| K | 21.77 | 0.078 | 19.5 | 96.4 | 1.55E+01 | 3.94E-03 |
| L | 21.78 | 0.071 | 36.3 | 97.1 | 1.51E+01 | 4.64E-03 |
| M | 21.83 | 0.055 | 57.8 | 98.2 | 1.53E+01 | 3.90E-03 |
| N | 21.83 | 0.065 | 83.0 | 97.4 | 1.54E+01 | 3.84E-03 |
| O | 21.70 | 0.073 | 95.5 | 95.6 | 1.53E+01 | 5.67E-03 |
| P | 21.78 | 0.139 | 98.8 | 92.4 | 1.64E+01 | 7.39E-03 |
| Q | 22.20 | 0.526 | 99.6 | 72.6 | 1.60E+01 | 1.15E-02 |
| R | 21.68 | 0.686 | 100.0 | 84.4 | 1.50E+01 | 1.74E-02 |

[26] Viewed individually, regardless of size or inclusion in fault zones, individual faults (Figure 6) strike north and dip steeply, with an average orientation of 176, 86W. Contouring the data with either Kamb (Figure 6) or Gaussian methods shows a well-developed cluster of poles consistent with this average orientation. Fault-related lineations such as striations and mineral fibers vary considerably in orientation, from steeply plunging to horizontal (Figure 6).

[27] Faults larger than grade V occur within 39 recognizable fault zones (Figure 3). Fault surfaces and slickenlines within each zone were averaged to produce an average plane and lineation for each fault zone (Figure 6c). Viewing the faults as average sites and omitting the smallest faults does not change the overall pattern of their orientation: most faults, regardless of size, strike north and dip steeply with steep to gently plunging lineations.

[28] Slip direction was determined for 24 fault zones from the average slickenline for that zone and from rare kinematic indicators such as fault steps and offset markers. Dip-slip faults are the most common type recognized, with 16 fault zones showing dip slip and two showing oblique slip (Figure 6). On average, the dip-slip faults strike north and dip nearly vertically, similar to both the average individual faults and the fault zones. The sense of dip slip is not well constrained: one fault zone recorded normal slip and another showed dextral-normal slip. The magnitude of dip slip cannot be determined. Rare truncated veins and dikes require many meters of dip slip on the larger (grade III and larger), but a general absence of restorable markers precludes estimates of slip magnitude. Nevertheless, the width and intensity of the deformation suggest the larger fault zones accommodated significant dip slip. Strike-slip faulting was recognized in six fault zones; four of these are dextral (Figure 6). The small number of strike-slip faults precludes meaningful statistical analysis, but we note that most strike-slip faults strike northwest, in contrast to the average northerly strike of the fault population as a whole.

### 4.4. Paleomagnetic Results

#### 4.4.1. Quottoon Remanence

[29] Figure 7 shows how samples from the Quottoon pluton responded to stepwise AF and thermal demagnetization. The remanence in most samples was hardly affected by AF treatment (up to 40 mT) or by subsequent thermal demagnetization up to the Curie temperature of magnetite (580°C). The sample behavior illustrated in the figures is typical; the arithmetic sum of remanence components removed by these treatments was usually less than 30% of the total sample remanence. Almost all the sample demagnetization occurred during heating from 580°C to just over 680°C. During these high-temperature steps, the magnetization of most samples decayed linearly toward the origin, and it was straightforward to define characteristic remanent magnetization directions.

[30] Figure 7 (d, g, and j) shows that high-temperature remanence loss usually peaked at two temperatures, one near 600°C and the other much closer to 680°C, the Curie temperature of pure hematite. In most cases, the magnetizations lost at these two temperatures had nearly the same orientation. Striking exceptions occurred in four samples from site 8Q127 where the lower blocking temperature (Tb) component was at a high angle (in two cases nearly antiparallel) to the higher Tb component. In sample 8Q127-2, for example, thermal demagnetization to 552°C had no effect on the sample's remanence ($D$ = 264, $I$ = 35), but at temperatures between 552°C and 585°C, the west down component was removed revealing an antiparallel component that was approximately half as large. In a second sample from this site (8Q129), there is evidence of three components associated with narrow and distinct Tb ranges centered on 570°C, 600°C, and 680°C.

[31] The very high coercivity and blocking temperatures of characteristic component from the Quottoon is strong evidence that iron-rich titanohematite is the predominant remanence carrier. This interpretation is supported by thin-section observations (Appendix A) showing that large grains consisting primarily of hematite-ilmenite intergrowths are the predominant opaque mineral. Previous work [*Gehrels and Boghossian*, 2000; *Rusmore et al.*, 2001, 2005] established that the Quottoon pluton intruded previously deformed metamorphic rocks of the Central Gneiss Complex and cooled through temperatures near 600°C between

**Figure 6.** Stereonets showing orientation of mafic dikes and brittle faults on Douglas Channel. All plots are equal area, lower hemisphere. (a) Mafic dikes. Stars indicate dated dikes. White contours are >8 times the standard deviation ($\sigma$) above expected count of uniform density. (b) Individual fault planes and slickenlines. Black area on Kamb plot represents density 10–12 times $\sigma$ above expected count. (c) Orientation and size of fault zones on Douglas Channel; symbols scaled relative to size of fault zone. (d) Faults zones with known slip or age relative to mafic dikes. Symbols scaled relative to size of fault zone. (right plot) Fault zones older than dikes shown in black; fault zones younger than dikes shown in gray.

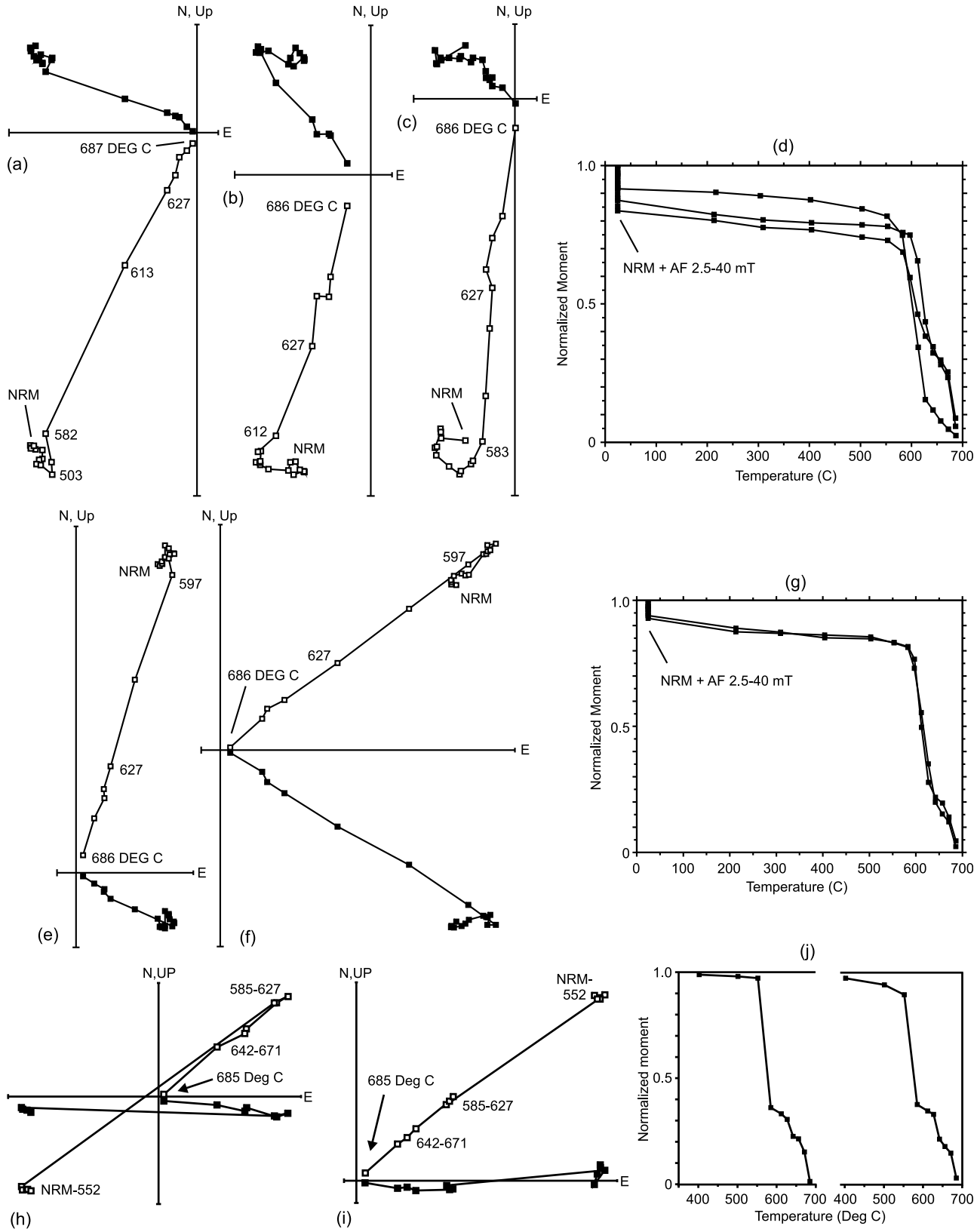
N, Up
E
687 DEG C
(a)
627
613
NRM
582
503
(b)
686 DEG C
627
612
NRM
(c)
686 DEG C
627
NRM
583
(d)
Normalized Moment
NRM + AF 2.5-40 mT
Temperature (C)
(e)
NRM
597
627
686 DEG C
(f)
597
NRM
627
686 DEG C
(g)
Normalized Moment
NRM + AF 2.5-40 mT
Temperature (C)
N,UP
585-627
642-671
685 Deg C
NRM-552
(h)
(i)
NRM-
552
685 Deg C
585-627
642-671
(j)
Normalized moment
Temperature (Deg C)

**Figure 7**

**Table 3.** Site Mean Remanence Summary[a]

| Site | Dg | Ig | $N$ | $k$ | $\alpha_{95}$ | Unit |
|---|---|---|---|---|---|---|
| 8Q001 | 302.3 | 66.7 | 7 | 161.8 | 4.8 | Quottoon |
| 8Q008 | 307 | 64.5 | 7 | 220.2 | 4.1 | Quottoon |
| 8Q022 | 272.7 | 64.6 | 7 | 167.6 | 4.7 | Quottoon |
| 8Q029 | 102.9 | −54.6 | 7 | 62.7 | 7.7 | Quottoon |
| 8Q036 | - | - | - | - | - | Quottoon |
| 8Q043 | 125.7 | −53.9 | 7 | 307 | 3.5 | Quottoon |
| 8Q050 | 341.9 | 83.1 | 6 | 1935 | 1.5 | Quottoon |
| 8Q057 | - | - | - | - | - | Quottoon |
| 8Q064 | 48.5 | 85.3 | 7 | 206.9 | 4.2 | Quottoon |
| 8Q078 | 42.7 | 82.2 | 7 | 154.5 | 4.9 | Quottoon |
| 8Q085 | 325.1 | 84.3 | 6 | 273.5 | 4.1 | Quottoon |
| 8Q092 | 131.5 | −72.4 | 5 | 263.1 | 4.7 | Quottoon |
| 8Q099 | 127 | −51.2 | 5 | 245.2 | 4.9 | Quottoon |
| 8Q106 | 125.7 | −34.2 | 6 | 185.5 | 4.9 | Quottoon |
| 8Q113 | - | - | - | - | - | Quottoon |
| 8Q120 | 290.2 | 37.7 | 5 | 79.8 | 8.6 | Quottoon |
| 8Q127 | 106.6 | −41.1 | 7 | 94 | 6.3 | Quottoon |
| 9M035 | - | - | - | - | - | Quottoon |
| 9M042 | 160.6 | −68.7 | 7 | 862.5 | 2.1 | Quottoon |
| 8Q015 | 1.7 | 75.5 | 7 | 331.0 | 3.3 | dike |
| 8Q071 | 119.8 | −84.0 | 7 | 85.2 | 6.6 | dike |
| 9M001 | 18.1 | 73.7 | 6 | 220.7 | 4.5 | dike |
| 9M008 | 14.5 | 73.9 | 7 | 188.4 | 4.4 | dike |
| 9M015[b] | 317.9 | 56.2 | 7 | 44.7 | 9.1 | dike |
| 9M022 | 2.3 | 70.2 | 6 | 313.7 | 3.8 | dike |
| 9M028[c] | 345.5 | 79.1 | 4 | 199.9 | 6.5 | dike |
| 9M049 | 113.0 | −54.1 | 6 | 48.1 | 9.8 | dike |
| 9M056 | - | - | - | - | - | dike |
| 9M063[b] | 338.7 | 64.2 | 4 | 129.8 | 8.1 | dike |
| 9M070 | - | - | - | - | - | dike |
| 9M077 | - | - | - | - | - | dike |

[a]Dg and Ig, declination and inclination (geographic coordinates) of site-mean remanence direction; $N$, number of samples directions averaged; $k$ and $\alpha_{95}$, precision parameter and radius of 95% confidence interval of *Fisher* [1953] on site-mean direction.
[b]Three of seven are inverted reversed components.
[c]Site not used for tectonic interpretations.

59 and 55 Ma without penetrative deformation. The magnetic remanence of the Quottoon is therefore Paleocene in age and postdates all the poleward tectonic transport posited by the "Baja BC" hypothesis [*Cowan et al.*, 1997; *Irving et al.*, 1985]. Cooling rates during acquisition of the remanence were high, but not more than ~100°C/Ma. [*Rusmore et al.*, 2001], implying that remanence acquisition took at least several hundred Ma, even at sites where the blocking temperature range was only a few tens of degrees. This inference is consistent with the observation of both normal and reverse polarity remanence (sometimes in the same specimen) and further implies that the site-mean remanence directions have averaged out the ancient geomagnetic secular variation.

[32] Table 3 and Figure 8 show site-mean results for 15 of the 19 sites in the Quottoon. We were unable to isolate a characteristic remanence in samples from the remaining four sites. Judged by the site-mean inclination, seven of the sites were magnetized when the geomagnetic field had reverse polarity and eight when the field was normal, but most directions are far from the expected early Tertiary field direction. Four of the normal polarity sites had very steep (>82°) inclinations and so their declinations are not well constrained. For the remaining sites, however, the mean declinations are an average of 49° counterclockwise of the direction expected at this locality. The inclinations range from 40° shallow to 11° steep compared to the expected direction, with the average inclination about approximately 7° shallower than expected. As described in Appendix B, these anomalous remanence directions cannot be explained by magnetic anisotropy related to the widely developed magmatic foliation in the Quottoon. Instead, we ascribe differences between expected and observed site-mean directions to local-to-regional scale structural rotations such as block tilting and oroclinal bending as described in more detail below.

#### 4.4.2. Miocene Dikes Remanence

[33] Figure 9 shows typical orthogonal vector demagnetization diagrams for samples from the Miocene dikes. Some samples such as those illustrated in Figures 9a and 9b of the figure exhibited linear decay to the origin after removal of a relatively minor low-coercivity or low-Tb component that was clearly secondary. The characteristic remanence was typically reduced to about 15% the natural remanent magnetization (NRM) and the surviving component was usually oriented in the same direction. In a majority of samples, however, very large low-coercivity and low-blocking temperature components made it difficult to cleanly isolate the characteristic remanences. For sample 9M059 in Figure 9c, a peak AF field of 20 mT was sufficient to remove more than half the sample's remanence, but 70 mT was insufficient to isolate the highest coercivity component of the sample's magnetization. Thermal demagnetization of a companion specimen from the same sample (Figure 9d) demonstrated that the low-coercivity component also had a low Tb (i.e., less than 200°C). The component that was apparently untouched by the AF demagnetization was completely removed by thermal demagnetization, suggest-

**Figure 7.** Demagnetization behavior of samples from the Quottoon pluton. The seven leftmost plots are orthogonal vector demagnetization diagrams of (a) 8Q006 (NRM intensity = $2.32 \times 10^{-2}$ A/m), (b) 8Q027 (NRM intensity = $8.03 \times 10^{-2}$ A/m), (c) 8Q090 (NRM intensity = $1.20 \times 10^{-2}$ A/m), (e) 8Q098 (NRM intensity = $2.58 \times 10^{-1}$ A/m), (f) 8Q107 (NRM intensity = $5.06 \times 10^{-2}$ A/m), (h) 8Q127-2 (NRM intensity = $2.59 \times 10^{-2}$ A/m), and (i) 8Q129-2 (NRM intensity = $1.03 \times 10^{-1}$ A/m). Samples in the first five plots were subjected to six levels of AF demagnetization(up to a peak field strength of 40 mT) followed by 12 or 13 steps of thermal demagnetization in air; the last two plots are thermal demagnetization only. Solid (open) symbols represent vector endpoints projected onto the horizontal (vertical) plane. The rightmost plots (d, g, and j) show the decrease in linearized remanence moment versus temperature for the same three samples. The starting moment (set arbitrarily equal to 1) is the arithmetic sum of the vector moments removed during the demagnetization steps plus the final moment. The multiple demagnetization steps plotting at room temperature in Figures 7d and 7g show the moments removed by stepwise AF demagnetization to 40 mT.

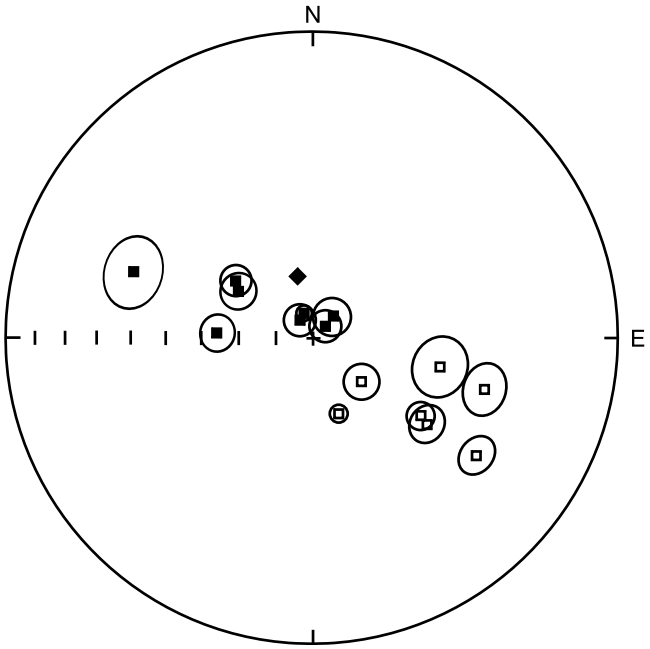


**Figure 8.** Equal area plot of site-mean directions (squares) and 95% confidence regions from the Quottoon pluton. Solid (open) symbol plots on lower (upper) hemisphere. Expected Paleocene field direction shown with diamond. Lower hemisphere equal area plot.

ing that it was carried by a high-coercivity hydrous iron oxide mineral, perhaps goethite. Sample 8Q077 (Figure 9e) responded similarly to thermal demagnetization (an average moment loss of 65% at 200°C), although the high Tb component from this sample has a very different orientation than that in 9M059. The low-coercivity components measured within weeks after collection from six samples at this site are consistently oriented and average to a direction well within a degree of the direction predicted for this location by the 2005 IGRF model. This observation strongly suggests this component is a very young viscous remanent magnetization.

[34] The site-mean directions are listed in Table 3 and plotted on an equal-area net in Figure 9f. Of the twelve sites we collected, only seven yielded site-mean directions. At three sites, we were unable to isolate any remanence components via stepwise demagnetization, and at two other sites only four of seven samples yielded a usable direction. We list the results for the latter two sites in Table 3 but do not include the site-mean directions in further analysis. Of the seven usable sites, five have steep inclinations and declinations close to north-south. These directions are close to both the average field for the last million years and to the Middle Miocene field inferred from the apparent polar wander curve for North America. Except for the single site recording reverse polarity, these site-mean directions are also very close to the present-day field. The other two sites have directions which are shallower than and counterclockwise of any average field direction expected at this site for the last 20 Ma.

[35] The remanent magnetization of the dikes was likely acquired quickly during rapid cooling of the dikes at ~20 Ma. Field evidence of rapid near-surface cooling includes chilled margins and abundant vesicles. The dikes intruded rocks that had cooled to about 250°C–300°C by 48 Ma and were near 70°C at 10 Ma [*Farley et al.*, 2001; *Friedman et al.*, 2001; *Gareau*, 1991; *Roddick*, 1970; *Rusmore et al.*, 2005]. Thus, it is probable that the dikes acquired their characteristic remanence over a time scale that was short (i.e., months to years) with respect to that of the geomagnetic secular variation.

## 5. Discussion

### 5.1. Patterns and Age of Deformation Along Transect

[36] Synthesis of the AHe ages, structural data, and paleomagnetic results reveals the style and spatial patterns of deformation along this transect as the transform margin formed and matured. Contrasting deformational histories along the transect define two adjacent regions shown on Figure 2: the core of the orogen and, to the southeast, the eastern flank of Queen Charlotte basin. Deformational events in these regions are discussed below and summarized in Table 4.

#### 5.1.1. Orogen Core

[37] Following initiation of the transform margin at circa 50 Ma, oroclinal bending is the oldest deformation recorded in the core of the orogen on our transect. This bend, referred to as the Hawkesbury Warp [*Roddick*, 1970], is most visibly expressed as a ~50° CCW deviation in the Quottoon pluton and adjacent Coast shear zone from the regional northwest trend (Figure 1) [*Roddick*, 1970; *Rusmore et al.*, 2005]. *Symons* [1977] attributed strongly counter-clockwise rotated paleomagnetic declinations in the Quottoon pluton to formation of the Hawkesbury Warp. Our new paleomagnetic and structural results help define the extent, age, and, when compared to regional deformation patterns, the origin of the orocline.

[38] The new paleomagnetic results from the Quottoon can be grouped into two domains comprising sites that are adjacent and have similar declinations (Figures 4 and 10). We interpret these rotation domains as representing crustal blocks that experienced similar but distinct deformations. The four sites at the northeast end of the Quottoon exposure (8Q022, 8Q029, 8Q120, and 8Q127) have similar declinations (283 ± 7.5) that average 63° clockwise of the expected direction ($D$ = 346.4, $I$ = 73.1, $\alpha_{95}$ = 3°, calculated from the North American Paleocene pole of *Beck and Housen* [2003]). We refer to this group of sites as rotation domain 1 (RD1). Of the remaining sites, six (8Q001, 8Q008, 8Q043, 8Q092, 8Q099, and 8Q106) have declinations (306.5° ± 3.0°) that are 40° clockwise of the expected direction. We group these sites into the rotation domain 2 (RD2) along with four nearby sites (8Q050, 8Q064, 8Q078, 8Q085) with inclinations so steep that the declinations are not well constrained. Site 9M042, well south of both rotation domains, has the expected direction and so shows no evidence of the large-scale rotation affecting the other sites.

[39] The paleomagnetically defined rotations of 40° to 63° closely bracket the 50° rotation seen geologically and by

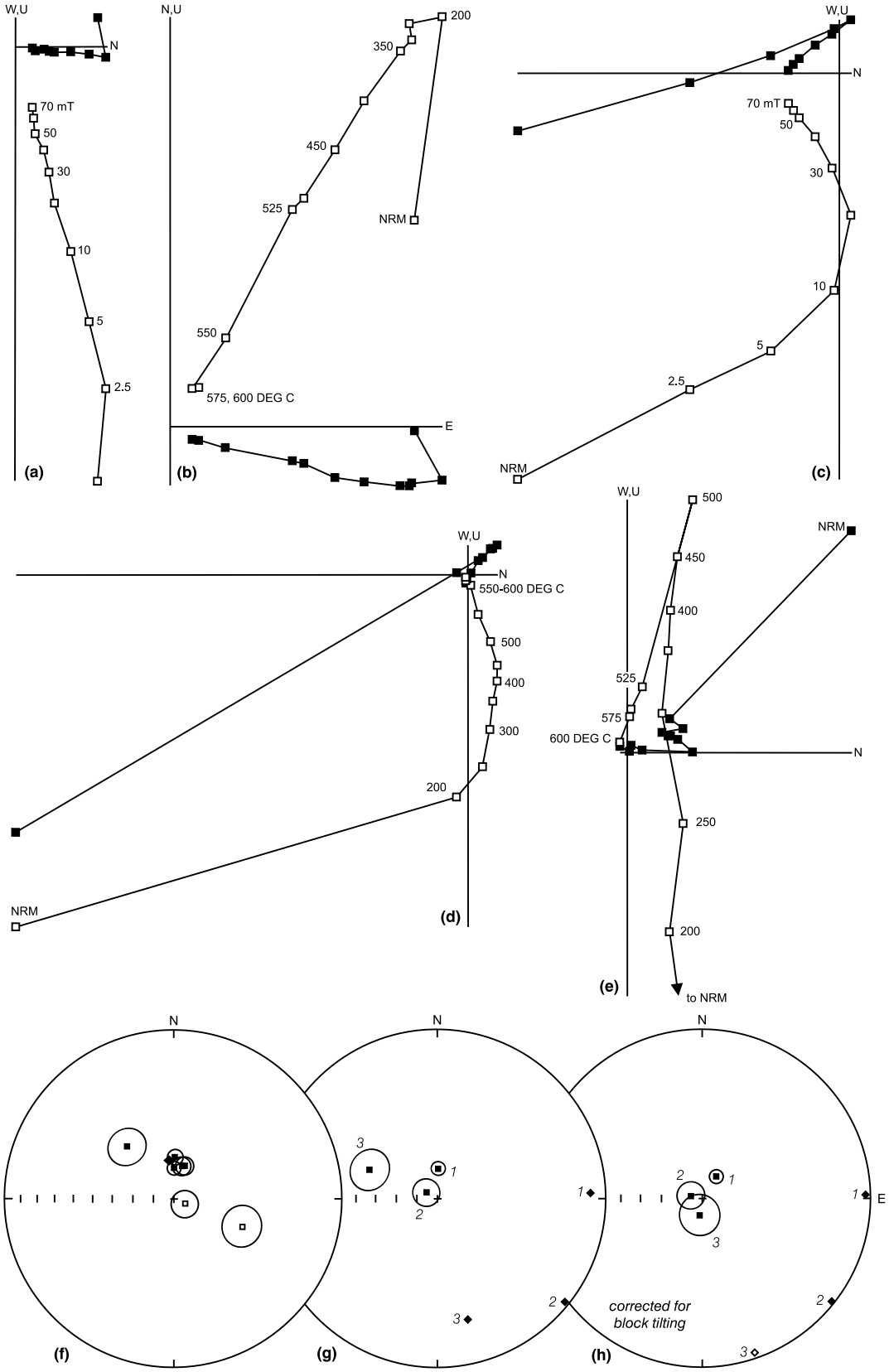
W,U
N
70 mT
50
30
10
5
2.5
(a)
N,U
200
350
450
525
550
NRM
575, 600 DEG C
E
(b)
W,U
N
70 mT
50
30
10
5
2.5
NRM
(c)
W,U
N
550-600 DEG C
500
400
300
200
NRM
(d)
W,U
500
NRM
450
400
525
575
600 DEG C
N
250
200
to NRM
(e)
N
(f)
N
3
1
2
3
(g)
N
1
1
E
2
3
corrected for
block tilting
2
3
(h)

**Figure 9**

**Table 4.** Deformational Events on Transect

| | Orogen Core | Eastern Flank of QC Basin |
|---|---|---|
| ~50–20 Ma | North striking normal faults, rotation of Quottoon pluton and surrounding rocks to form Hawkesbury Warp<br>NE striking brittle faults | Graben formation at ~25–20 Ma |
| ~20 Ma | Intrusion of mafic dikes | |
| Post-20 Ma | NW striking dextral strike-slip faults | Continued graben growth until at least 9 Ma<br>Normal faulting on graben flanks |
| Post-5 Ma | Local tilting of small crustal domains<br>Rapid exhumation [*Farley et al.*, 2001] | |

*Symons* [1977], and the site (9M042) outside of the Hawkesbury Warp appears unrotated. These results strongly suggest that this zigzag shape of the Quottoon has resulted from large-scale deformation of an initially linear feature. There is a substantial (>20°) difference in rotation between RD1 and RD2, a value which is large compared to the declination variation observed within either domain (Figure 10). The sharp difference in rotation between domains occurs over ~10 km between sites 8Q029 and 8Q106, suggesting that the crust in this area behaved as large (on the order 10 km) rigid blocks during the bending.

[40] This paleomagnetically defined differential rotation provides a way to show that formation of the Hawkesbury Warp preceded intrusion of the dikes at ~20 Ma. The test involves a comparison of the orientations of dikes in the two rotation domains defined on the basis of the Quottoon paleomagnetism. The 32 dikes in RD1 (after correction for younger block tilting discussed below) have a mean restored strike of 55.0° (with 95% confidence limits of −9.6°/+11.7° calculated via a bootstrap resampling scheme). The mean strike of 72 dikes in RD2 is identical (55.2°, −8.8°/+8.9°). Correcting the dike orientations for the 23.2°of differential vertical axis rotation between the two domains would leave the mean strikes of two sets of dikes distinct at a very high (>95%) confidence level. This observation suggests that the formation of the Hawkesbury Warp took place before the dikes were intruded at about ~20 Ma.

[41] Most of the brittle faults in the orogen core are also likely to be older than about 20 Ma. Direct evidence of pre-20 Ma faulting comes from the mafic dikes. Orogen-perpendicular faults, now northeast striking, are intruded by undeformed mafic dikes in three locations. Although only a few of these faults were observed, they likely acted as conduits for intrusion of the northeast striking dikes and so have been obscured. The NE striking and nearly vertical orientation of these faults is consistent with formation as extensional faults in an E-W striking sinistral shear couple during formation of the Hawkesbury Warp.

[42] The most common faults, those that strike north and are commonly dip slip, were not found interacting with dikes, but AHe dating suggests that significant dip slip on these faults is older than 20 Ma. Along most of Douglas Channel, sea-level ages AHe ages vary smoothly from ~10 to 2 Ma and correlate with changes in topography [*Farley et al.*, 2001]. Elevation profiles from three locations spanning 80 km across the orogen record existence of a partial retention zone between about 30 and 10 Ma [*Farley et al.*, 2001]. Slow steady exhumation of ~0.22 mm/yr occurred from about 10 to <4 Ma, when exhumation rates increased about 70% [*Farley et al.*, 2001]. The pattern of sea level ages and consistent results from the widely separated elevation profiles show that most of Douglas Channel is underlain by a coherent crustal block that has not experienced significant vertical disruption since at least 20 Ma [*Farley et al.*, 2001]. If our impression that the width and intensity of fabric development within the dip-slip fault zones signal significant slip, then the north striking, dip-slip faults are older than ~20 Ma. Because many of these dip-slip faults cut the 58 Ma Quottoon pluton, they likely formed while the transform margin was active. Striking 40°–45° clockwise from the transform boundary, they are favorably oriented to be normal faults kinematically linked to the Queen Charlotte transform.

[43] Mafic dikes are cut by northwest striking faults in five faults zones, four of which show unconstrained strike slip or a component of dextral slip. These relations suggest

**Figure 9.** Paleomagnetic results for Miocene dikes from Douglas Channel. (a–e) Orthogonal vector demagnetization diagrams; see Figure 7 for explanation. (a) AF demagnetization of 9M008-1 (NRM intensity = $2.32 \times 10^{-1}$ A/m); (b) thermal demagnetization of 9M054-2 (NRM intensity = $1.46 \times 10^{-2}$ A/m); (c) AF demagnetization of 9M059-1 (NRM intensity = $5.00 \times 10^{-1}$ A/m); (d) thermal demagnetization of a second specimen from the same sample (NRM intensity = $3.70 \times 10^{-1}$ A/m); (e) thermal demagnetization of 8Q077-2 (NRM intensity = $4.84 \times 10^{-1}$ A/m). The north versus up point (solid) for the NRM is omitted to show more detail of the behavior after the 200°C step. The intensity for the 200°C step is $6.07 \times 10^{-2}$ A/m. (f) Equal area plot of site-mean remanence directions (squares) and 95% confidence regions for 7 Miocene dikes. (g) Squares are remanence directions for sites (1) 8Q015, (2) 8Q071, and (3) 9M049, with (2) and (3) inverted through the origin. Diamonds are poles to dike orientations. (h) Same data after correction for tilts inferred from paleomagnetism of the Quottoon pluton. Expected Paleocene field direction shown with diamond. Solid (open) symbol plots on lower (upper) hemisphere.

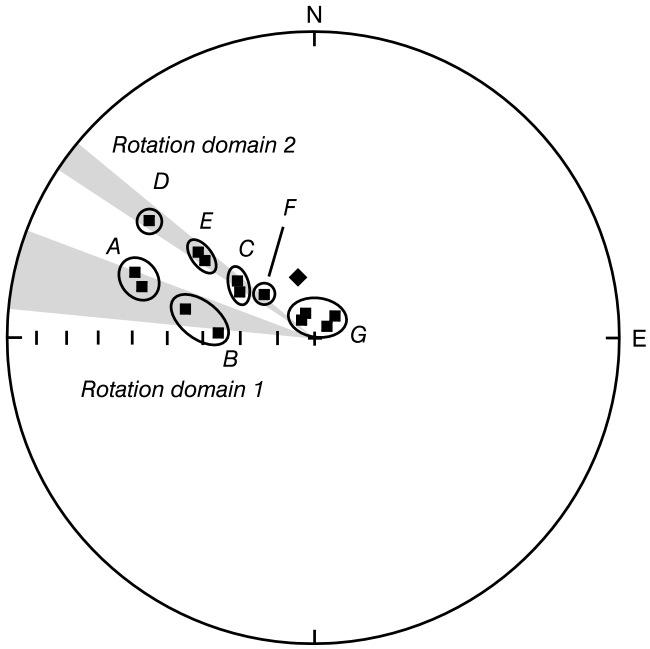


**Figure 10.** Paleomagnetic directions defining rotation and tilt domains in the Quottoon pluton. Squares show paleomagnetic site-mean directions with reverse polarity directions inverted through the origin. Shaded sectors indicate average declination (+ standard deviation) of sites in two rotation domains. Ovals enclose sites grouped into tilt domains A through G. Expected Paleocene field direction for Douglas Channel locality shown with diamond. Lower hemisphere equal area plot.

that the NW striking faults were active after 20 Ma but do not preclude initiation of this set of faults prior to 20 Ma. Their age, orientation, and hints of dextral slip suggest these strike-slip faults are synthetic to the Queen Charlotte transform.

[44] A final phase of tilting in the core of the orogen is revealed by paleomagnetic results, dike orientations, and AHe ages. Tilting is shown by paleomagnetic site-mean inclinations in the Quottoon pluton that are more variable than site-mean declinations and do not correspond to the rotation domains. The sites group naturally into seven small domains (most ~1 km across), TDA through TDG (Figure 4, 10, and Table 5), each comprising adjacent sites with approximately the same apparent tilt. Because the tilting postdates oroclinal bending, it is appropriate to undo the CCW rotation to compare the site-mean direction of each tilt domain to the Paleocene North American reference direction (i.e., by 63° for tilt domains in RD1 and 40° for those in RD2). Table 5 shows the results of this analysis. Tilts range from 38.9° to 1.6° and all inferred tilt axes are close to horizontal. The sense of tilting in five domains (TDA through TDE) is up to the west to west northwest. One domain (TDF) is essentially untilted, and TDG is 15.3° up to east southeast. The magnitude and direction of tilting is constant over a distance of 10 km in TDG, but elsewhere significant variations in the tilt occur between sites less than 1 km apart (e.g., 8Q029 and 8Q106). Along Douglas Channel from TDB (at the ENE end) to TDG (at the WSW end), the inferred tilts increase from 14° to 39° and then decrease to −15° (where positive tilts are up to NW and negative tilts are up to the SE). The data thus allow the possibility that the tilting is continuously variable; unlike the rotation domains, the tilt domains may not correspond to discrete crustal blocks. Much denser sampling of the pluton is needed to determine whether the tilting reflects rigid block deformation or a more continuous crustal deformation.

[45] The age of this tilting is constrained by the orientations and remanence of the Miocene dikes and AHe ages. Dikes that cut the Quottoon pluton and lie near paleomagnetic sites were assigned to tilt and rotation domains. Of the 231 dikes examined in this study, about half fit this criterion. Their mean strike is 56° with 95% confidence limits of (−7.0°, +6.4°) and a mean dip of 81.5°NW (−3.5°, +4.1°) as estimated via a bootstrap resampling scheme. If crustal tilting took place after intrusion of the dikes, then the dikes can be restored to their pre-tilting orientations using the rotations listed in Table 5. This restoration leaves the mean strike unchanged but brings the mean dip to 85.3° (−3.9°, +3.8°). The restored dip is just within the 95% confidence limit on the in situ value, but just outside the limits at the 90% confidence level. The restored dip is therefore different from the in situ value at a high degree of probability. More importantly, this restoration brings the mean dip closer to the value (90°) that would be expected for a population of undisturbed dikes. We interpret this observation as evidence that the tilting followed intrusion of the dikes.

**Table 5.** Tilt Domains[a]

| Name | Sites | Dec | Inc | RD | Azm | Plg | Tilt | Azm* | Plg* | tilt* |
|---|---|---|---|---|---|---|---|---|---|---|
| TDA | 120, 127 | 288.4 | 39.4 | 1 | 200.2 | −2.1 | 33.8 (W) | 184.7 | 16.1 | 43.4 |
| TDB | 022, 029 | 278.6 | 59.7 | 1 | 183.8 | 2.8 | 13.5 (W) | 157.7 | 16.7 | 28.2 |
| TDC | 001, 008 | 304.7 | 65.6 | 2 | 211.1 | 1.7 | 7.5 (W) | 173.0 | 16.8 | 16.0 |
| TDD | 106 | 305.7 | 34.2 | 2 | 215.5 | 0.3 | 38.9 (NW) | 206.6 | 13.1 | 43.9 |
| TDE | 043, 099 | 306.4 | 52.6 | 2 | 216.3 | 0.1 | 20.5 (NW) | 196.2 | 14.8 | 26.4 |
| TDF | 092 | 311.5 | 72.4 | 2 | 282.7 | −15.5 | 1.6 (N) | 152.9 | 16.5 | 10.3 |
| TDG | 050, 064, 078, 085 | 009.6 | 84.9 | 2 | 19.7 | −5.0 | 15.3 (E) | 67.4 | −2.7 | 12.4 |

[a]Name, tilt domain designation (120 = 8Q120); Sites, paleomagnetic sites included in tilt domain. Estimated ancient field direction (before tectonic rotation) is Dec = 346.4, Inc = 73.1 (for site at 53.8°N, 231.0°E, Paleoecene NAM pole from *Diehl et al.* [1983]). Dec, Inc, mean paleomagnetic declination and inclination of tilt domain, reversely magnetized sites inverted through origin. RD, local vertical axis rotation domain. RD1 is rotated 63.3° CCW; RD2 is rotated 39.9° CCW. Azm, Plg, Tilt, azimuth and plunge of inferred tilt axis, and amount of CW rotation about axis assuming tilt followed vertical axis rotation (direction toward uptilted end of crustal block). Azm*, Plg*, Tilt*, same for single rotation that takes expected direction to tilt domain mean.

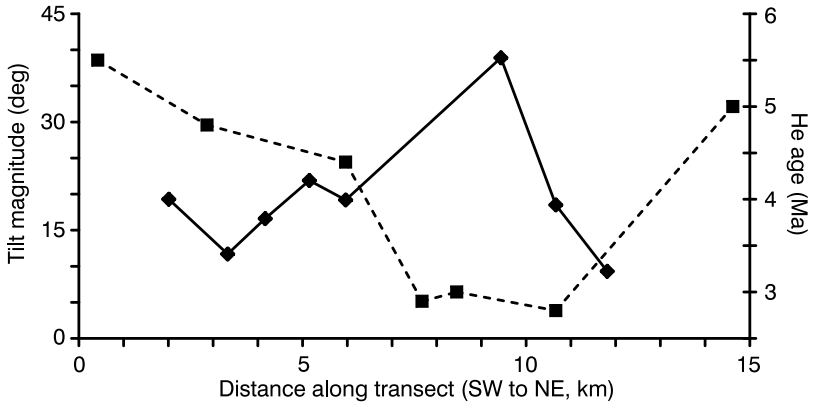


**Figure 11.** Paleomagnetically inferred tilt magnitude (solid line) and apatite (U-Th)/He ages (dashed) from *Farley et al.* [2001] across the Coast Mountains orogen core at Douglas Channel. Data are projected onto a SW to NE line along the northwest channel shoreline beginning 2 km southwest of paleomagnetic site 8Q078. Tilts at all but the two southwesternmost sites are NW side up.

[46] A second line of evidence is provided by the paleomagnetism of the dikes themselves. Of the dikes that yielded reliable remanence directions, only three intruded the Quottoon intrusion. All three were close to paleomagnetic sites in the Quottoon and were assigned to the corresponding tilt domain (8Q015 to TDC; 8Q071 to TDG; and 9M049 to TDD). Applying the tilts in each of these domains (Table 5) to the dikes brings the three dikes closer to vertical, as is the case for the larger dike population, and produces a tighter cluster of remanence directions (Figures 9g and 9h). The change in the remanence directions is shown by an increase in the precision parameter $k$ from 18.4 to 52.4, which is significant at the 83% confidence level. The remanence of the dikes thus suggests that tilting followed intrusion of the dikes.

[47] Independent evidence suggesting a young age for the tilting comes from the AHe results reported in *Farley et al.* [2001], a portion of which are plotted on Figure 11. As discussed by *Farley et al.* [2001], sea-level AHe ages on a transect perpendicular to the trend of the range form a V-shaped pattern with the youngest ages (under 3 Ma) coinciding with range's topographic axis. As shown on Figure 11, the minimum in sea-level AHe ages also correlates with the region where paleomagnetically inferred tilting is greatest. This observation suggests that the tilting is associated with the differential exhumation apparent in the AHe ages and therefore very young, perhaps ongoing. *Farley et al* [2001] suggest that rapid glacial erosion may have driven this exhumation. If so, the tilting may be an example of erosionally driven crustal deformation and thus unrelated to the transform margin.

#### 5.1.2. Eastern Flank of the Queen Charlotte Basin

[48] The fairly stable mid-Miocene history of the orogen core contrasts sharply with a record of significant Miocene faulting and graben formation on the eastern flank of the Queen Charlotte basin. AHe ages range from 9 to 57 Ma and vary in abrupt steps, rather than the much smaller and gradual variations seen in the orogen core (Figure 2).

[49] The largest differences in AHe ages coincide with the Grenville Channel and Principe-Laredo faults, signaling a Miocene episode of faulting (Figures 1 and 2). Ages jump from Middle and Late Miocene (14–9 Ma) to Eocene (47 Ma) across the Grenville Channel fault, previously interpreted as a Mesozoic sinistral ductile shear [*Chardon et al.*, 1999]. These AHe ages suggest that the Grenville Channel fault was reactivated in Middle Miocene time, when it accommodated significant NE side-up slip. Similarly, the change from 49 to 27 Ma on Campania Island to 15 Ma on Trutch Island across the trace of the Principe-Laredo fault is consistent with Middle Miocene or younger SW side-up slip on two fault strands. The relatively older AHe ages from Gil and Campania Islands suggest they form a more coherent down-dropped block in the center of a graben bounded by the Principe-Laredo and Grenville Channel faults. The relative crustal stability from ~50 to 23 Ma implied by the slow cooling of the samples from Campania Island suggests that graben formation did not begin until Early Miocene time. Comparison of AHe ages from the down-dropped block suggest it may have been tilted. At the smaller grain size, 99MR-62 from the southwestern part of graben is about 10 Ma younger than the sample from the northwestern edge of the graben, 99MR-65. The ages are nearly identical at the largest grain size of overlap between the two samples. This result implies that the graben floor experienced modest southwest side-up tilting, most likely during graben formation.

[50] Minor faults disrupt both flanks of the graben (Figure 2). On the northeastern flank, two faults are recognized from disruptions in AHe age patterns and exposures of faults (Figure 2). A NW striking fault is inferred east of the Grenville Channel fault, where AHe ages abruptly drop from 14 to 10 Ma and two northwest striking, dip slip, grade II fault zones are exposed. Similarly, a short dip-slip fault probably underlies the southernmost segment of Douglas Channel, where AHe ages differ by as much as 6 Ma across the channel and several dip-slip, north, and northeast striking faults are exposed along the shore. Apparently, rocks

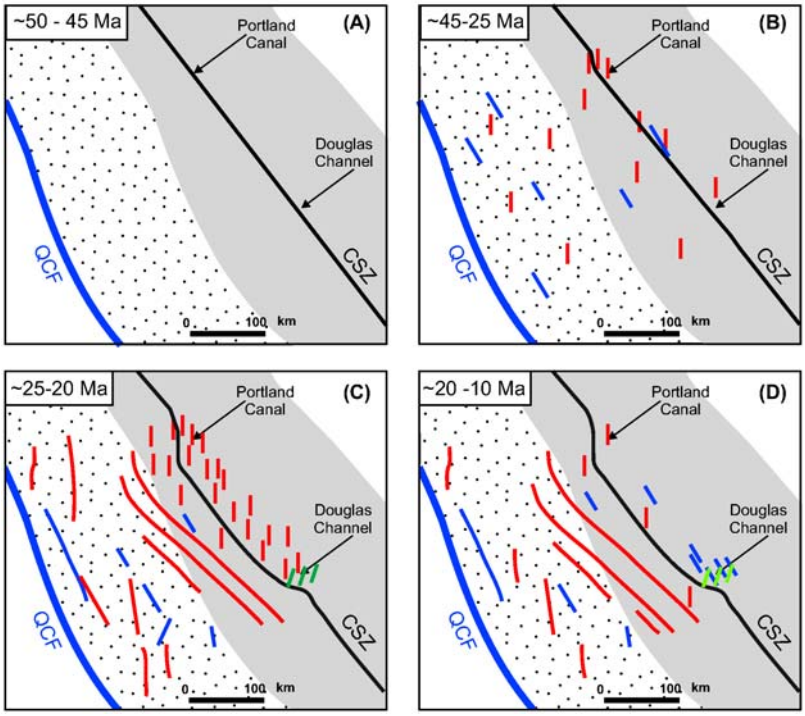


**Figure 12.** Schematic maps showing interpreted evolution of the transform margin. The extinguished Cretaceous magmatic arc is shown in light gray; the forearc is stippled. The Coast shear zone (CSZ) is inactive. Dextral faults are shown in blue; normal faults in red. (a) Shortly after initiation the transform boundary, shown as the Queen Charlotte fault (QCF). The evolution of the QCF is not well known so it is shown without change in all maps. (b) Widespread normal faulting affects the margin far as 250 km inboard of the transform. Dextral faulting documented at 30 Ma east of CSZ [*Davidson et al.*, 2003]; other occurrences are inferred. (c) Main phase of normal faulting opens Queen Charlotte Basin, initiates graben formation on its eastern flank, and in the orogen core deflects the CSZ, forming prominent bends in orogenic trends. Local northeast striking faults (shown in dark green) on Douglas Channel form in response to bending. (d) Decreased faulting in QCB, continued graben formation on eastern flank of QCB. Intrusion of mafic dike swarm (shown in light green) on Douglas Channel, followed by northwest striking dextral faulting.

west of the fault were down-dropped and tilted down to the north after 7 Ma.

[51] The southwestern flank of the graben is exposed on Trutch Island, where two AHe ages are ~15 Ma. The eastern sample is 300 m higher than the western one, perhaps indicating a few degrees of northeast side-up tilting about a NW striking axis. A NE side-up Miocene fault most likely lies along the western side of Trutch Island, separating the 15 Ma ages from a 57 Ma age on the western shore. This fault may be the southern continuation of a normal fault imaged just offshore from Banks Island, where it is the eastern boundary of the West Banks graben [*Rohr and Dietrich*, 1992].

[52] Overall, results from this transect show that the early stages of formation of the transform margin affected the core of the orogen more than 250 km from the present transform boundary. Deformation of the orogen core between about 50 and 20 Ma included oroclinal bending to produce the Hawkesbury Warp and development of northeast and north striking dip-slip faults before intrusion of a northeast striking mafic dike swarm at ~ 20 Ma. As the margin matured, the locus of extensional faulting migrated toward the transform, manifested by formation of the graben between the Grenville and Principe-Laredo faults after ~23 Ma and continuing until at least 9 Ma. During this time, dextral strike-slip faulting affected the core of the orogen, but significant normal faulting was absent. Local tilting of small domains in the core mimics the pattern of post-4 Ma exhumation shown by AHe ages [*Farley et al.*, 2001] and may be related erosionally driven exhumation rather than transform-margin processes.

### 5.2. Regional Response to Transform Boundary

[53] Integration of our results with previous work in the Coast Mountains and adjacent Queen Charlotte Basin reveals shifting patterns of transform-related deformation within the continental margin (Figure 12). Following initiation of the transform around 50 Ma, normal and dextral faults affected the continental margin as much as 250 km inboard from the active transform for about 300 km along the strike of the orogen. Significant normal faulting is

inferred to have produced about 30% extension near Portland Canal around 50 Ma (Figure 12), with extension decreasing to the NW and SE [*Butler et al.*, 2001a]. Continued extension on Portland Canal is recorded by more than 300 mapped mafic dikes ranging from 39 to <22 Ma and north striking extensional Tertiary brittle faults [*Evenchick et al.*, 1999]. Compared to normal faults on Douglas Channel, these faults are wider and disrupt geologic map patterns, so they probably accommodated more extension. Another example of post-50 Ma faults far from the transform occurs along the Skeena River, about halfway between Portland Canal and Douglas Channel (Figures 1 and 12). Northwest striking dextral faults were active at 30 Ma [*Davidson et al.*, 2003], and post-50 Ma normal faults at this location strike NNE; both orientations are kinematically compatible with the Queen Charlotte fault. Reverse faults strike NW to NE; their origin is uncertain [*Davidson et al.*, 2003]. The amount of extension accommodated by the normal faults is unknown, but, unlike Portland Canal, paleomagnetic results do not indicate crustal tilting, suggesting less extension occurred at the Skeena River [*Butler et al.*, 2001a]. Post-50 Ma extension within the core of the orogen thus appears to have been greatest at Portland Canal.

[54] This difference in net extension may have caused the oroclinal bending seen in the Hawkesbury Warp and a complementary bend 300 km northwest near the mouth of Portland Canal (Figure 1), where the Coast shear zone and Paleocene plutons along it bend to the north. Only in these bends does the 1200+ km long Coast shear zone deviate from a remarkably consistent northwest strike [*Ingram and Hutton*, 1994; *Klepeis et al.*, 1998; *McClelland et al.*, 1992; *Rusmore et al.*, 2001]. We infer that the two bends mark the southern and northern boundaries of a more highly extended domain, with the Coast shear zone serving as a passive strain marker for extension northeast of it. Deflection of the Coast shear zone is greatest (~40 km) at Portland Canal, where geologic evidence supports the greatest post-50 Ma extension east of the Coast shear zone.

[55] This extended domain lies within previously extended continental crust, now exposed as the Central Gneiss Complex (Figure 1). Between ~55 and 52 Ma, rapid ductile extension exhumed and cooled mid-crustal rocks of the Central Gneiss Complex [*Andronicos et al.*, 2003; *Hollister*, 1982; *Hollister and Andronicos*, 2006; *Klepeis and Crawford*, 1999; *Rusmore et al.*, 2005]. This spatial coincidence suggests that the previously extended crust served to localize and/or focus extension in the core of the orogen as the transform margin evolved.

[56] Brittle faulting also affected the margin closer to the transform, with Tertiary dextral and extensional faults visible on the Queen Charlotte Islands [*Lewis et al.*, 1991], but the age and distribution of these structures are obscured by intense extension during formation of the Queen Charlotte Basin between ~25 and 20 Ma [*Dehler et al.*, 1997; *Rohr and Currie*, 1997; *Woodsworth*, 1991]. Generally, north striking normal faults formed the basin and are interpreted as linked to northwest striking dextral faults within the basin and the Queen Charlotte transform [*Dehler et al.*, 1997; *Rohr and Currie*, 1997; *Woodsworth*, 1991]. Focused rifting may have formed the main part of the basin in about 5 Ma, with ~76% extension [*Dehler et al.*, 1997].

[57] Formation of the Queen Charlotte Basin was coincident with initiation of graben formation on the eastern flank of the basin. The newly recognized graben between the Grenville and Principe-Lardeo faults on our transect records disruption of the basin margin beginning about 23 Ma. We conclude that this graben is the southeastern continuation of a graben recognized on seismic images [*Hollister et al.*, 2008; *Rohr and Dietrich,* 1992; *Rohr et al.*, 2000]. Northwest of our transect the Principe-Laredo fault bounds a 2.5 km deep half-graben with Miocene down-to-the-east normal motion [*Rohr and Dietrich*, 1992; *Rohr et al.*, 2000]. *Hollister et al.* [2008] interpret the Principle-Laredo fault and an unnamed fault to the east as a large, relatively young, graben (Figure 1) located above midcrustal ductile extensional shear zones and conclude that the northeastern margin of the basin records at least 30% extension. Connection to the graben recognized on our transect makes this structure more than 200 km long, compatible with significant extension.

[58] The peak of extension and oroclinal bending in the core of the orogen can only be constrained to 50–20 Ma; however, the intensity of extension in the Queen Charlotte Basin between 25 and 20 Ma makes this a likely age for extension in the core. Accordingly Figure 12c shows the peak of normal faulting and oroclinal bending at this time. Northeast striking faults on Douglas Channel are interpreted as resulting from the bending.

[59] Extension waned across the continental margin following the main phase of basin formation (Figure 12d), as the zone of active extension narrowed and shifted toward the transform. After ~20 Ma, normal faulting in the core of the orogen ended on our transect, although dextral faults were active. Graben growth continued on the eastern flank of the Queen Charlotte Basin until at least 9 Ma. Within the basin itself, normal and strike-slip faulting continued through the Miocene [*Lewis et al.*, 1991; *Dehler et al.*, 1997].

[60] The patterns of deformation within the continental margin reinforce the view that plate boundary motion was accommodated by kinematically linked normal and strike-slip faults [*Dehler et al.*, 1997; *Hollister et al.*, 2008; *Morozov et al.*, 2001]. Notably, this deformation affects the continental margin far inboard of the plate boundary. Strict spatial partitioning of the deformation into dextral and normal fault domains is not observed; however, extension dominated the orogen during a brief period (~25–20 Ma), with the greatest extension in the present Queen Charlotte Basin. Thus, it appears that formation of the transform margin and slab window caused initially widespread deformation, and with time, the locus of extension shifted toward the transform, became more focused and intensified to form the Queen Charlotte Basin. Coeval dextral faulting continued in the core of the orogen, 250 km inboard of the transform.

### 5.3. Bearing on the Baja BC Controversy

[61] Controversy over the Cretaceous paleogeography of western British Columbia revolves around interpretation of anomalously shallow paleomagnetic inclinations from Cretaceous plutonic rocks [e.g., *Butler et al.*, 2001b; *Cowan et*

*al.*, 1997; *Irving*, 1985; *Irving et al.*, 1985; *Mahoney et al.*, 1999; *Wyld et al.*, 2006]. Critical to the argument is whether the anomalous inclinations are caused by uniform northeast side-up tilting of plutons along ~1000 km of the coast orogen and Washington Cascades, rather than latitudinal translation [e.g., *Cowan et al.* 1997]. Significant Cretaceous and Neogene northeast side-up tilting has been proposed to explain anomalous inclinations on the eastern flank of the Queen Charlotte Basin [*Butler et al.*, 2001a, 2006; *Butzer et al.*, 2004]. Tilting of this character is not evident in our results; it is neither widespread nor uniform in sense or amount. For example, the paleomagnetic inclinations of small, kilometer-scale blocks in the core of the orogen have been affected by tilting that is variable in direction (though predominantly west northwest side up) and magnitude. No northeast side-up tilts are observed. AHe ages signal local tilting on the eastern flank of the Queen Charlotte Basin, but here too, the direction of tilting is variable, including north, northeast, and southwest side-up tilts. Because the sense, amount, and distribution of Neogene tilting is highly variable, it cannot explain the regionally consistent pattern of shallow paleomagnetic inclinations. Thus, if uniform northeast side-up tilting affected Mesozoic plutons in western British Columbia, it occurred prior to 50 Ma, was subsequently modified by more variable local tilting, and is unlikely to have produced a widespread systematic bias to paleomagnetic inclinations as proposed by *Butler et al.* [2001a].

### 5.4. Comparison to Gulf of California

[62] Comparison of the development the Queen Charlotte and Baja California transform margins shed some light on the role of strain partitioning in the development of transform boundaries in continental crust. Two fundamental differences in the boundaries frame the comparison: the development of the Queen Charlotte transform margin spans nearly 50 million years; about 3 times longer than formation of the transform margin in Baja California. Additionally, plate motions have been generally parallel to the Queen Charlotte transform [*Doubrovine and Tarduno*, 2008] and transtensional in Baja California [*Lonsdale*, 1989; *Stock and Molnar*, 1988]. Despite these differences, in both locations the transform boundary localized in continental crust, accompanied by significant rifting and basin formation. In the early stages of transform development (circa 50–25 Ma) strain inboard of the Queen Charlotte transform was widespread, with normal and strike-slip faulting developed across the region. Strain within the continent does not appear to be partitioned at this time, and the lack of throughgoing and recognizable faults from this period suggests that most plate motion was taken up along the transform itself. Regional partitioning of strain increased during formation of the Queen Charlotte basin, when normal faulting seems to have dominated the continental margin for about 5 Ma. These patterns suggest that plate motion largely controlled the patterns of strain; motion was parallel to the plate boundary, and most strain appears to have taken place on the transform itself. Compared with the margin in Baja California; the pattern of deformation is more akin to the models calling for transtensional deformation on the Gulf of California system [*Fletcher et al.*, 2007] rather that strongly partitioned rifting in the Gulf and strike slip near the former trench [e.g., *Stock and Hodges*, 1989]. In any case, the development of coeval normal and strike-slip faults in the Coast Mountains far from the transform lends support to the idea that some plate motion may have been accommodated by strike-slip faulting on the eastern margin of the Gulf of California [*Fletcher et al.*, 2007; *Gans*, 1997; *Oskin and Stock*, 2003].

[63] Regardless of how they evolved initially, both transforms ultimately localized in continental crust, and extension related to the transform affected the margin far from the original trench [*Lonsdale*, 1989; *Stock and Hodges*, 1989]. In Baja, however, the transform is now localized in the older arc; in British Columbia, it developed in the former forearc. In both areas, the zone of active extension narrowed and migrated toward the transform with time. In Baja, the Gulf Extension Province flanks the active rift, and the rift itself appears to have narrowed and stepped westward with time [*Aragon-Arreola and Martin-Barajas*, 2007; *Umhoefer et al.*, 2002], a pattern similar to localization of extension in Queen Charlotte Basin following widespread extension. Perhaps most intriguing, both margins underwent significant crustal extension prior to initiation of the transform margin [e.g. *Andronicos et al.*, 2003; *Gans*, 1997; *Klepeis and Crawford*, 1999; *Nourse et al.*, 1994; *Rusmore et al.*, 2005]. These similarities suggest that development of a transform in continental crust is aided by previous crustal extension and that initially widespread extension associated with the transform narrows as the margin develops.

## 6. Conclusions

[64] Deformation related to the Queen Charlotte fault extension initially affected a wide swath of the continental margin; normal and dextral faults linked to the transform developed as far as 250 km inboard of the plate boundary. Localization of extension in previously extended continental crust in the core of the orogen suggests that prior crustal thinning helped establish the widespread transform-related extension. The zone of active extension narrowed and migrated toward the transform through time, leading to formation the Queen Charlotte Basin about 20–30 Ma after the initiation of the transform margin. Tilting of crustal blocks throughout this region varied in direction, so systematic Tertiary extension is not a likely mechanism to produce the anomalous paleomagnetic inclinations seen in plutons in the Coast Mountains. Comparison to the Gulf of California leads us to speculate that significant continental extension influences subsequent localization and development of transform margins within continental crust.

## Appendix A: Polished Thin-Section Observations

[65] Examination of polished thin sections in transmitted and reflected light provides insight into the source of the remanence in the Quottoon pluton (Figure A1). Some samples contain large (apparent widths of order 1 mm) opaque magmatic grains (Figure A1a) which are largely a

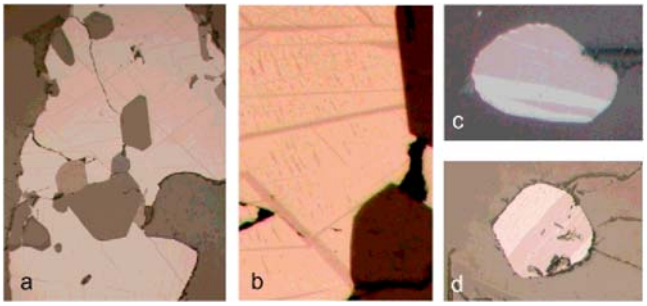


**Figure A1.** Photomicrographs showing opaque grains in samples from the Quottoon pluton. (a) Large opaque grain (appearing bright) in reflected light from sample 8Q053. Image is 432 $\mu$m wide. (b) Close-up of the central portion of grain from (a) in reflected light. Bright mineral hosting lamellae is hematite. Large dark lamellae with straight edges are rutile; smaller wavy lamellae are ilmenite. Image is 75 $\mu$m wide. (c) Small rounded opaque grain in plagioclase from sample 8Q082. Image is 60 $\mu$m wide and is in reflected light. Opaque grain contains both ilmenite (dark) and hematite (bright). (d) Small subeuhedral opaque grain in plagioclase from sample 8Q058. Image is 235 $\mu$m wide and is in reflected light. Upper left portion of grain is hematite (bright) with small ilmenite lamellae (dark); lower right portion of grain is mostly ilmenite with small hematite lamellae.

highly reflective and anisotropic mineral, presumably iron-rich ilmenohematite (referred to here simply as "hematite"). These large grains invariably exhibit straight-edged, translucent exsolution lamellae of rutile (which form a "blitz" texture) and shorter, wavy lamellae that are opaque, anisotropic, and have lower reflectivity than the hematite host (Figure A1b). These lamellae, presumably titanium-rich ilmenohematite ("ilmenite"), produce the familiar "tiger stripe" texture in the regions of these large grains between the rutile lamellae. Figures A2c and A2d show two examples of much smaller, slightly rounded euhedral to subhedral opaque grains that occur as inclusions in silicate hosts. These grains display tiger stripe texture arising from both ilmenite lamellae (in hematite) and hematite lamellae (in ilmenite). Rutile lamellae are present in some of these grains. Both these kinds of grains appear to have crystallized directly from the melt.

[66] A third kind of grain, shown in Figure 2 occurs as blades on grain boundaries of hornblende and biotite grains or on cleavage planes in biotite. No exsolution lamellae were visible in these grains. We identify these blades, which are highly reflective, anisotropic, and a deep red color on thin, translucent edges, as hematite. Their occurrence on silicate grain boundaries and cleavage planes suggests that these grains grew via solid state diffusion of iron from the adjacent silicate mineral after the pluton was solid, cooling, but still at high temperature.

[67] For the magmatic grains (either discrete or included in silicate), which show ilmenite-hematite exsolution textures, some of the remanence may be a lamellar magnetism, a high-temperature (~572°C [*McEnroe et al.*, 2005]) CRM originating in contact layers between the two phases [*Robinson et al.*, 2002]. Lamellar magnetism has been invoked [*Robinson et al.*, 2002] as an explanation for ilmenohematite-bearing plutonic or metamorphic rocks with unusually strong (i.e., of order 10 A/m) magnetizations. The remanence of the Quottoon tonalite samples is much lower (of order 0.1 A/m) and so the lamellar magnetism hypothesis is plausible but not required.

## Appendix B: Effect of Magnetic Anisotropy on the Quottoon Remanence

[68] Most samples from the Quottoon pluton are coarse grained, so an intrinsic grain level anisotropy might not be averaged out. To assess this possibility, we determined the anisotropy of a remanence induced in the laboratory (IRM) that provides a good analog [*Stephenson et al.*, 1986] for the anisotropy of TRM (presumably the primary remanence of the pluton). The procedure, described in the work of *Bogue et al.* [1995], involves imparting 20 and 40 mT IRMs to a sample in three orthogonal directions and inferring the anisotropy from differences in these remanences. We also

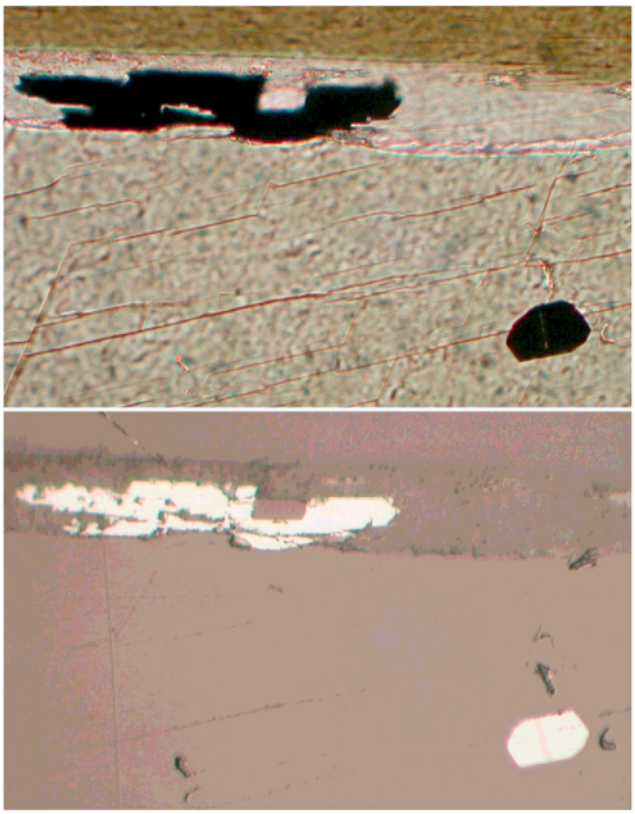

**Figure A2.** Photomicrographs (transmitted light above and reflected light below) showing two kinds of opaque grains from sample 8Q132. Image is 184 $\mu$m wide. Opaque grain at top left in each image is hematite on grain boundary between bitotite (above) and hornblende (below). Small subhedral grain at lower right is hematite with large rutile and smaller ilmenite lamellae.

**Table A1.** Sample Locations[a]

| Sample | Elevation (m) | UTM East | UTM North | Sample Type |
|---|---|---|---|---|
| 99MR-31 | 0 | 550458 | 5924667 | AHe |
| 99MR-55 | 0 | 452902 | 5879117 | AHe |
| 99MR-58 | 297 | 454702 | 5881517 | AHe |
| 99MR-60 | 0 | 459501 | 5879417 | AHe |
| 99MR-61 | 0 | 462601 | 5886517 | AHe |
| 99MR-62 | 0 | 463351 | 5891817 | AHe |
| 99MR-63 | 0 | 476901 | 5895417 | AHe |
| 99MR-65 | 0 | 482661 | 5902517 | AHe |
| 99MR-68 | 0 | 472876 | 5920057 | AHe |
| 98MR-69 | 0 | 497755 | 5957342 | Hb Ar-Ar |
| 99MR-03 | 0 | 483501 | 5937567 | Hb Ar-Ar |
| 8Q001 | 0 | 506825 | 5953892 | paleomagnetic |
| 8Q008 | 0 | 506700 | 5954242 | paleomagnetic |
| 8Q015 | 0 | 506700 | 5954242 | paleomagnetic |
| 8Q022 | 0 | 505800 | 5960792 | paleomagnetic |
| 8Q029 | 0 | 505000 | 5959917 | paleomagnetic |
| 8Q043 | 0 | 501005 | 5957442 | paleomagnetic |
| 8Q050 | 0 | 493970 | 5964377 | paleomagnetic |
| 8Q057 | 0 | 495425 | 5959857 | paleomagnetic |
| 8Q064 | 0 | 497755 | 5957342 | paleomagnetic |
| 8Q071 | 0 | 497755 | 5957342 | paleomagnetic |
| 8Q078 | 0 | 497500 | 5955537 | paleomagnetic |
| 8Q085 | 0 | 498120 | 5957042 | paleomagnetic |
| 8Q092 | 0 | 499095 | 5957077 | paleomagnetic |
| 8Q099 | 0 | 500195 | 5957197 | paleomagnetic |
| 8Q106 | 0 | 503600 | 5959817 | paleomagnetic |
| 8Q120 | 0 | 512960 | 5958242 | paleomagnetic |
| 8Q127 | 0 | 514299 | 5960142 | paleomagnetic |
| 9M001 | 0 | 486400 | 5944777 | paleomagnetic |
| 9M008 | 0 | 489125 | 5946517 | paleomagnetic |
| 9M015 | 0 | 501100 | 5952067 | paleomagnetic |
| 9M022 | 0 | 491675 | 5950617 | paleomagnetic |
| 9M028 | 0 | 541149 | 5923217 | paleomagnetic |
| 9M042 | 0 | 550458 | 5924667 | paleomagnetic |
| 9M049 | 0 | 504160 | 5958617 | paleomagnetic |
| 9M056 | 0 | 506660 | 5962292 | paleomagnetic |
| 9M063 | 0 | 508990 | 5964857 | paleomagnetic |
| 9M070 | 0 | 512510 | 5968042 | paleomagnetic |
| 9M077 | 0 | 520649 | 5973667 | paleomagnetic |

[a]Locations are NAD83, Zone 9N.

assessed the anisotropy of TRM in 14 Quottoon specimens that had been previously thermally demagnetized to 687°C. We imparted a TRM by heating and cooling samples to 687° C in a laboratory field of 50 μT oriented within a few degrees of each specimen's cylindrical axis. After measuring that TRM, samples were thermally demagnetized at 590°C to isolate the high-Tb portion of the TRM.

[69] Comparison of the site-mean remanence directions to the magmatic foliation present in the Quottoon pluton shows that site-mean remanence directions tend to lie near the magmatic foliation; 12 of the 15 are within 33° and 7 are within 13°. The magnetic anisotropy of the samples, however, suggests this relation is fortuitous. The AIRM in the Quottoon samples was substantial (averaging 1.32 if expressed as the ratio of the maximum to minimum susceptibility in the 20–40 mT coercivity fraction) but bore no clear spatial relationship to the magmatic layering measured at the sites. Furthermore, the AIRM was not consistently oriented within (or between) paleomagnetic sites and so did not have a significant effect on site-mean directions. In the TRM acquisition experiments, the average difference between the laboratory field and high Tb remanence directions was 5.9° ± 2.3°, far smaller than the large differences between the site-mean remanences and estimated ancient field directions. It was clear from the visual appearance of the samples that the laboratory heatings induced substantial alteration, especially dehydration of hornblende and biotite grains. It is quite possible therefore that part of the observed TRM deflection are associated with ferromagnetic material produced during this alteration. In short, there seems to be no significant rock magnetic expression of the magmatic foliation and so it is unlikely to be imparting any significant bias to site-mean remanence directions.

## Appendix C: Locations of Samples

[70] The locations of all samples analyzed in this study are shown in Table A1.

[71] **Acknowledgments.** This research was supported by NSF awards EAR 0310011, 9805124, and 9807740. We are grateful to all who helped us in the field: Bill Robinson provided excellent logistical support, and help from our field assistants Shannon Shula, Juliet Robinson, and Ron Karpilo was invaluable. Discussions with Carol Evenchick, George Gehrels, Lincoln Hollister, James Haggart, and Paul Umhoefer have shaped our thoughts on this topic over the years. Reviews by Associate Editor Paul Kapp and Michael Oskin greatly improved the manuscript.

## References

Anderson, R. G., and I. Reichenbach (1991), U-Pb and K-Ar Framework for Middle to Late Jurassic (172 – ~158 Ma) and Tertiary (46–27 Ma) Plutons in Queen Charlotte Islands, British Columbia, in *Evolution and Hydrocarbon Potential of the Queen Charlotte Basin, British Columbia*, edited by G. J. Woodsworth, pp. 59–87, Geol. Surv. of Can., Ottawa, Ont.

Andronicos, C. L., D. H. Chardon, L. S. Hollister, G. E. Gehrels, and G. J. Woodsworth (2003), Strain partitioning in an obliquely convergent orogen, plutonism, and synorogenic collapse: Coast Mountains Batholith, British Columbia, Canada, *Tectonics*, *22*(2), 1012, doi:10.1029/2001TC001312.

Aragon-Arreola, M., and A. Martin-Barajas (2007), Westward migration of extension in the northern Gulf of California, Mexico, *Geology*, 571–574.

Beck, M. E., and B. A. Housen (2003), Absolute velocity of North America during the Mesozoic from paleomagnetic data, *Tectonophysics*, *377*, 33–54.

Bogue, S. W., C. S. Gromme, and J. W. Hillhouse (1995), Paleomagnetism, magnetic anisotropy, and mid-cretaceous paleolatitude of the Duke Island (Alaska) ultramafic complex, *Tectonics*, *14*, 1133–1152.

Breitsprecher, K., D. J. Thorkelson, W. G. Groome, and J. Dostal (2003), Geochemical confirmation of the Kula-Farallon slab window beneath the Pacific northwest in Eocene time, *Geology*, *31*, 351–354.

Butler, R. F., G. E. Gehrels, M. L. Crawford, and W. A. Crawford (2001a), Paleomagnetism of the Quottoon plutonic complex in the Coast Mountains of British Columbia and southeastern Alaska: Evidence for tilting during uplift, *Can. J. Earth Sci.*, *38*, 1367–1385.

Butler, R. F., G. E. Gehrels, and K. P. Kodama (2001b), Baja British Columbia hypothesis, *GSA Today*, *11*, 4–10.

Butler, R. F., G. E. Gehrels, W. Hart, C. Davidson, and M. L. Crawford (2006), Paleomagnetism of Late Jurassic to mid-Cretaceous plutons near Prince Rupert, British Columbia, in *Paleogeography of the North American Cordillera: Evidence for and against Large-Scale Displacements*, Geological Association of Canada Special Paper 46, edited by J. W. Haggart, R. J. Enkin and J. W. H. Monger, pp. 171–200.

Butzer, C., R. F. Butler, G. E. Gehrels, C. Davidson, K. O'Connell, and M. L. Crawford (2004), Neogene tilting of crustal panels near Wrangell, Alaska, *Geology*, *32*, 1061–1064.

Chardon, D., C. L. Andronicos, and L. S. Hollister (1999), Large-scale transpressive shear zone patterns and displacements within magmatic arcs: The Coast Plutonic Complex, British Columbia, *Tectonics*, *18*, 278–292.

Clark, M., G. Maheo, J. Saleeby, and K. Farley (2005), The non-equilibrium landscape of the southern Sierra Nevada, California, *GSA Today*, *15*.

Cowan, D. S., M. T. Brandon, and J. I. Garver (1997), Geologic tests of hypotheses for large coastwise displacements - a critique illustrated by the Baja British Columbia controversy, *Am. J. Sci.*, *297*, 117–173.

Crawford, M. L., W. A. Crawford, and J. Lindline (2005), 105 million years of igneous activity, Wrangell, Alaska, to Prince Rupert, British Columbia, *Can. J. Earth Sci.*, *42*, 1097–1116.

Davidson, C., K. J. Davis, C. M. Bailey, C. H. Tape, J. Singleton, and B. Singer (2003), Age, origin, and significance of brittle faulting and pseudotachylyte along the Coast Shear Zone, Prince Rupert, British Columbia, *Geology*, *31*, 43–46.

Dehler, S. A., C. E. Keen, and M. M. Rohr (1997), Tectonics and thermal evolution of Queen Charlotte Basin: Lithospheric deformation and subsidence models, *Basin Res.*, *9*, 243–261.

Diehl, J., M. Beck Jr., S. Beske-Diehl, D. Jacobson, and B. Hearn Jr. (1983), Paleomagnetism of the Late Cretaceous-early Tertiary north-central Montana alkalic province, *J. Geophys. Res.*, *88*(B12), 10,593–10,609.

Doubrovine, P. V., and J. A. Tarduno (2008), A revised kinematic model for the relative motion between Pacific oceanic plates and North America since the Late Cretaceous, *J. Geophys. Res.*, *113*, B12101, doi:10.1029/2008JB005585.

Ehlers, T. A., K. A. Farley, M. E. Rusmore, and G. J. Woodsworth (2006), Apatite (U-Th)/He signal of large-magnitude accelerated glacial erosion, southwest British Columbia, *Geology*, *34*(9), 765–768.

Edwards, B. R., and J. K. Russell (1999), Northern Cordilleran volcanic province: A northern Basin and Range?, *Geology*, *27*, 243–246.

Edwards, B. R., and J. K. Russell (2000), Distribution, nature, and origin of Neogene-Quaternary magmatism in the northern Cordilleran Volcanic Province, Canada, *Geol. Soc. Am. Bull.*, *112*, 1280–1295.

Engebretson, D. C., A. Cox, and R. G. Gordon (1985), *Relative Motions between Oceanic and Continental Plates in the Pacific Basin*, *Special Paper 206.*, 59 p. Geol. Soc. Am., Boulder, CO.

Evenchick, C. A., M. L. Crawford, V. J. McNicoll, L. D. Currie, and P. B. O'Sullivan (1999), Early Miocene or Younger Normal Faults and Other Tertiary Structures in West Nass River Map Area, Northwest British Columbia, and Adjacent Parts of Alaska, in *Current Research 1999-A*, pp. 1–11, Geol. Surv. Canada, Ottawa, Ont.

Farley, K. A., R. A. Wolf, and L. T. Silver (1996), The effects of long alpha-stopping distances on (U-Th)/He Ages, *Geochim. Cosmochim. Acta*, *60*, 4223–4229.

Farley, K. A., M. E. Rusmore, and S. W. Bogue (2001), Post-10 Ma uplift and exhumation of the northern Coast Mountains, British Columbia, *Geology*, *29*, 99–102.

Fisher, R. A. (1953), Dispersion on a sphere, *Proc. R. Soc. London*, *A217*, 295–305.

Fletcher, J. M., M. Grove, D. Kimbrough, O. Lovera, and G. E. Gehrels (2007), Ridge-trench interactions and the neogene tectonic evolution of the Magdalena Shelf and southern Gulf of California: Insights from detrital zircon U-Pb ages from the Magdalena Fan and adjacent areas, *Geol. Soc. Am. Bull.*, *119*, 1313–1336.

Friedman, R. M., S. A. Gareau, and G. J. Woodsworth (2001), U-Pb dates from the Scotia-Quaal metamorphic belt, Coast Plutonic Complex, central-western British Columbia, in *Radiogenic Age and Isotopic Studies: Report 14*, *Geol. Surv. of Can.*, Current Research 2001-F9.

Gans, P. B. (1997), Large-magnitude Oligo-Miocene extension in southern Sonora: Implications for the tectonic evolution of Northwest Mexico, *Tectonics*, *16*, 388–408.

Gareau, S. A. (1991), The Scotia-Quaal metamorphic belt: A distinct assemblage with pre-early Late Cretaceous deformational and metamorphic history, Coast Plutonic Complex, British Columbia, *Can. J. Earth Sci.*, *28*, 870–880.

Gehrels, G. E., and N. D. Boghossian (2000), Reconnaissance Geology and U-Pb Geochronology of the West Flank of the Coast Mountains between Bella Coola and Prince Rupert, Coastal British Columbia, in *Tectonics of the Coast Mountains, Southeastern Alaska and Coastal British Columbia*, *Special Paper 343*, edited by W. C. McClelland, pp. 61–76, Geol. Soc. Am., Boulder, CO.

Haeussler, P. J., D. C. Bradley, R. E. Wells, and M. L. Miller (2003), Life and death of the resurrection plate: evidence for its existence and subduction in the northeastern Pacific in Paleocene-Eocene time, *Geol. Soc. Am. Bull.*, *115*, 867–880.

Hickson, C. (1991), The Masset Formation on Graham Island, Queen Charlotte Island, British Columbia, in *Evolution and Hydrocarbon Potential of the Queen Charlotte Basin, British Columbia*, *Paper 90-10*, edited by G. J. Woodsworth, pp. 305–324, Geol. Surv. of Can., Ottawa, Ont.

Hollister, L. S. (1982), Metamorphic evidence for rapid (2 mm/yr) uplift of a portion of the Central Gneiss Complex, Coast Mountains, B.C., *Can. Mineral*, *20*, 319–332.

Hollister, L. S., and C. L. Andronicos (2006), Formation of new continental crust in western British Columbia during transpression and transtension, *Earth Planet. Sci. Lett.*, *249*, 29–38.

Hollister, L. S., J. Diebold, and T. Das (2008), Whole crustal response to late Tertiary extension near Prince Rupert, British Columbia, *Geosphere*, 360–374.

House, M. A., K. A. Farley, and D. Stockli (2000), Helium chronometry of apatite and titanite using Nd-YAG laser heating, *Earth Planet. Sci. Lett.*, *183*, 365–368.

Hutchison, W. W. (1982), *Geology of the Prince Rupert-Skeena Map Area, British Columbia*, Memoir 394, 116 pp., Geol. Surv. of Can., Vancouver, B. C.

Hyndman, R. D., and T. S. Hamilton (1991), Cenozoic Relative Plate Motions Along the Northeastern Pacific Margin and Their Association with Queen Charlotte Area Tectonics and Volcanism, in *Evolution and Hydrocarbon Potential of the Queen Charlotte Basin, British Columbia*, *Paper 90-10*, edited by G. J. Woodsworth, pp. 107–126, Geol. Surv. of Can., Ottawa, Ont.

Ingram, G. M., and D. H. W. Hutton (1994), The Great Tonalite Sill: Emplacement into a contractional shear zone and implications for Late Cretaceous to Early Eocene Tectonics in Southeastern Alaska and British Columbia, *Geol. Soc. Am. Bull.*, *106*, 715–728.

Irving, E. (1985), Whence British Columbia?, *Nature*, *314*, 673–674.

Irving, E., J. G. Souther, and J. Baker (1992), Tertiary extension and tilting in the Queen Charlotte Islands, evidence from dyke swarms and their paleomagnetism, *Can. J. Earth Sci.*, *29*, 1878–1898.

Irving, E. G., G. J. Woodsworth, P. J. Wynne, and A. Morrison (1985), Paleomagnetic evidence for displacement from the south of the Coast Plutonic Complex, British Columbia, *Can. J. Earth Sci.*, *22*, 548–598.

Kirschvink, J. L. (1980), The least-squares line and plane and the analysis of palaeomagnetic data, *Geophys. J. Int.*, *62*, 699–718, doi:10.1111/j.1365-246X.1980.tb02601.x

Klepeis, K. A., and M. L. Crawford (1999), High-temperature arc-parallel normal faulting and transtension at the roots of an obliquely convergent orogen, *Geology*, *27*, 7–10.

Klepeis, K. A., M. L. Crawford, and G. Gehrels (1998), Structural history of the crustal-scale Coast shear zone north of Portland Canal, Southeast Alaska and British Columbia, *J. Struct. Geol.*, *20*, 883–904.

Lewis, P. D., J. W. Haggart, R. G. Anderson, C. J. Hickson, R. I. Thompson, J. R. Dietrich, and K. M. M. Rohr (1991), Triassic to Neogene Geologic evolution of the Queen-Charlotte Region, *Can. J. Earth Sci.*, *28*, 854–869.

Lonsdale, P. (1988), Paleogene history of the Kula Plate: Offshore evidence and onshore implications, *Geol. Soc. Am. Bull.*, *100*, 733–754.

Lonsdale, P. (1989), Geologic and tectonic history of the Gulf of California, in *The Geology of North America, N, The Eastern Pacific Ocean and Hawaii*, edited by E. L. Winterer, D. M. Hussong and R. W. Decker, Geol. Soc. Am., Boulder, Colo.

Madsen, J. K., D. J. Thorkelson, R. M. Friedman, and D. D. Marshall (2006), Cenozoic to Recent plate configurations in the Pacific Basin: Ridge subduction and slab window magmatism in western North America, *Geosphere*, *2*, 11–34.

Mahéo, G., J. Saleeby, Z. Saleeby, and K. A. Farley (2009), Tectonic control on southern Sierra Nevada topography, California, *Tectonics*, *28*, TC6006, doi:10.1029/2008TC002340.

Mahoney, J. B., P. S. Mustard, J. W. Haggart, R. M. Friedman, C. M. Fanning, and V. J. McNicoll (1999), Archean zircons in Cretaceous strata of the western Canadian Cordillera: The "Baja BC" hypothesis fails a "crucial test," *Geology*, *27*, 195–198.

Matmon, A., D. P. Schwartz, P. J. Haeussler, R. Finkel, J. J. Lienkaemper, H. D. Stenner, and T. E. Dawson (2006), Denali fault slip rates and Holocene-late Pleistocene kinematics of central Alaska, *Geology*, *34*, 645–648.

McClelland, W. C., G. E. Gehrels, S. D. Samson, and P. J. Patchett (1992), Structural and geochronologic relations along the western flank of the Coast Mountains batholith: Stikine River to Cape Fanshaw, Central Southeastern Alaska, *J. Struct. Geol.*, *14*, 475–489.

McEnroe, S. A., et al. (2005), Lamellar Magnetism: Effects of interface versus exchange interactions of nanoscale exsolutions in the ilmenite-hematite system, *J. Phys. Conference Series*, *17*, 154–167.

Morozov, J. B., S. B. Smithson, L. S. Hollister, and J. B. Diebold (1998), Wide-angle seismic imaging across accreted terranes, southeastern Alaska and Western British Columbia, *Tectonophysics*, *299*, 281–296.

Morozov, I. B., S. B. Smithson, J. R. Chen, and L. S. Hollister (2001), Generation of new continental crust and terrane accretion in southeastern Alaska and western British Columbia: Constraints from P- and S-wave wide-angle seismic data (Accrete), *Tectonophysics*, *341*, 49–67.

Nourse, J. A., T. H. Anderson, and L. T. Silver (1994), Tertiary metamorphic core complexes in Sonora, Northwestern Mexico, *Tectonics*, *13*, 1161–1182.

Oskin, M., and J. Stock (2003), Pacific-North America plate motion and opening of the upper Delfin Basin, Northern Gulf of California, Mexico, *Geol. Soc. Am. Bull.*, *115*, 1173–1190.

Prims, J., K. P. Furlong, K. M. M. Rohr, and R. Govers (1997), Lithospheric structure along the Queen Charlotte margin in Western Canada: Constraints from flexural modeling, *Geo-Mar. Lett.*, *17*, 94–99.

Reiners, P. W., and K. A. Farley (2001), Influence of crystal size on apatite (U-Th)/He thermochronology: An example from the Bighorn Mountains, Wyoming, *Earth Planet. Sci. Lett.*, *188*, 413–420.

Robinson, P., R. J. Harrison, S. A. McEnroe, and R. B. Hargraves (2002), Lamellar magnetism in the haematite-ilmenite series as an explanation for strong remanent magnetization, *Nature*, *418*, 517–520.

Roddick, J. A. (1970), *Douglas Channel-Hecate Strait Map-Area, British Columbia*, *Paper 70-42*, 56 pp., Geol. Surv. of Can., Ottawa, Ont.

Rohr, K., and J. R. Dietrich (1991), Deep Seismic Reflection Survey of the Queen Charlotte Basin, British Columbia, in *Evolution and Hydrocarbon Potential of the Queen Charlotte Basin, British Columbia*, *Paper 90-10*, edited by G. J. Woodsworth, pp. 127–134, Geol. Surv. of Can., Ottawa, Ont.

Rohr, K. M., and L. Currie (1997), Queen Charlotte Basin and Coast Mountains: Paired belts of subsidence and uplift caused by a low-angle normal fault, *Geology*, *25*, 819–822.

Rohr, K. M. M., and J. R. Dietrich (1992), Strike-slip tectonics and development of the Tertiary Queen Charlotte Basin, Offshore Western Canada: Evidence from seismic reflection data, *Basin Res.*, *4*, 1–19.

Rohr, K. M. M., M. Scheidhauer, and A. M. Trehu (2000), Transpression between two warm mafic plates: The Queen Charlotte fault revisited, *J. Geophys. Res.*, *105*, 8147–8172.

Rusmore, M. E., G. Gehrels, and G. J. Woodsworth (2001), Southern continuation of the Coast Shear Zone and Paleocene strain partitioning in British Columbia-Southeast Alaska, *Geol. Soc. Am. Bull.*, *113*, 961–975.

Rusmore, M. E., G. J. Woodsworth, and G. E. Gehrels (2005), Two-stage exhumation of midcrustal arc rocks, Coast Mountains, British Columbia, *Tectonics*, *24*, TC5013, doi:10.1029/2004TC001750.

Souther, J. G., and A. M. Jessop (1991), Dyke Swarms in the Queen Charlotte Islands, British Columbia, and Implications for Hydrocarbon Exploration, in *Evolution and Hydrocarbon Potential of the Queen Charlotte Basin, British Columbia*, *Paper 90-10*, pp. 465–487, Geol. Surv. of Can., Ottawa, Ont.

Spencer, J. E., and W. R. Normark (1979), Tosco-Abreojos fault zone: A Neogene transform plate boundary within the Pacific Margin of Southern Baja California, Mexico, *Geology*, *7*, 554–557.

Stephenson, A., S. Sadikun, and D. K. Potter (1986), A theoretical and experimental comparison of the anisotropies of magnetic-susceptibility and remanence in rocks and minerals, *Geophys. J. R. Astron. Soc.*, *84*, 185–200.

Stock, J., and P. Molnar (1988), Uncertainties and implications of the Late Cretaceous and Tertiary position of North America relative to the Farallon, Kula, and Pacific Plates, *Tectonics*, *7*, 1339–1384.

Stock, J. M., and K. V. Hodges (1989), Pre-Pliocene Extension around the Gulf of California and the Transfer of Baja California to the Pacific Plate, *Tectonics*, *8*, 99–115.

Symons, D. T. A. (1977), Geotectonics of Cretaceous and Eocene plutons in British Columbia: A Paleomagnetic fold test, *Can. J. Earth Sci.*, *14*, 1246–1262.

Umhoefer, P. J., L. Mayer, and R. J. Dorsey (2002), Evolution of the Margin of the Gulf of California near Loreto, Baja California Peninsula, Mexico, *Geol. Soc. Am. Bull.*, *114*, 849–868.

Wheeler, J. O., and P. McFeely (1991), Tectonic Assemblage Map of the Canadian Cordillera and Adjacent Parts of the United States of America, Map 1712A, Geol. Surv. of Can.

Woodsworth, G. J. (1991), Neogene to Recent Volcanism Along the East Side of Hecate Strait, British Columbia, in *Evolution and Hydrocarbon Potential of the Queen Charlotte Basin, British Columbia*, *Paper 90-10*, edited by G. J. Woodsworth, pp. 325–336, Geol. Surv. of Can., Ottawa, Ont.

Wyld, S. J., P. J. Umhoefer, and J. E. Wright (2006), Reconstructing Northern Cordilleran Terranes Along Known Cretaceous and Cenozoic Strike-Slip Faults: Implications for the Baja British Columbia Hypothesis and Other Models, in *Paleogeography of the North America Cordillera: Evidence for and against Large-Scale Displacements*, Geological Association of Canada Special Paper 46, edited by J. W. Haggart, R. J. Enkin, and J. W. H. Monger, pp. 277–298.

S. W. Bogue, K. Dodson, and M. E. Rusmore, Department of Geology, Occidental College, Los Angeles, CA 90041, USA. (rusmore@oxy.edu)

K. A. Farley, Division of Geological and Planetary Sciences, California Institute of Technology, MS 170-25, Pasadena, CA 91125, USA.

G. J. Woodsworth, Geological Survey of Canada, 625 Robson St., Vancouver, BC V6B 5J3, Canada.